Chapter 8
Attractive and Repulsive Casimir–Lifshitz Forces, QED Torques, and Applications to Nanomachines

Federico Capasso, Jeremy N. Munday and Ho Bun Chan

Abstract This chapter discusses recent developments in quantum electrodynamical (QED) phenomena, such as the Casimir effect, and their use in nanomechanics and nanotechnology in general. Casimir–Lifshitz forces arise from quantum fluctuations of vacuum or more generally from the zero-point energy of materials and their dependence on the boundary conditions of the electromagnetic fields. Because the latter can be tailored, this raises the interesting possibility of designing QED forces for specific applications. After a concise review of the field in the introduction, high precision measurements of the Casimir force using MicroElectroMechanical Systems (MEMS) are discussed. Applications to nonlinear oscillators are presented, along with a discussion of their use as nanoscale position sensors. Experiments that have demonstrated the role of the skin-depth effect in reducing the Casimir force are then presented. The dielectric response of materials enters in a non-intuitive way in the modification of the Casimir–Lifshitz force between dielectrics through the dielectric function at imaginary frequencies $\varepsilon(i\xi)$. The latter is illustrated in a dramatic way by experiments on materials that can be switched between a reflective and a transparent state (hydrogen switchable mirrors) and by a large reduction of the Casmir force between a gold sphere and a thick gold film, when the latter is replaced by an indium tin oxide (ITO) thick film. Changing the electromagnetic density of states by altering the shape of the interacting surfaces on a scale comparable to their separation is an effective method to tailor Casimir–Lifshitz forces. Measurements of the latter between a

F. Capasso (✉)
School of Engineering and Applied Sciences, Harvard University, Cambridge, MA 02138, USA

J. N. Munday
Department of Electrical and Computer Engineering, University of Maryland, College Park, Maryland 20742, USA

D. Dalvit et al. (eds.), *Casimir Physics*, Lecture Notes in Physics 834,
DOI: 10.1007/978-3-642-20288-9_8,

silicon surfaces nanostructured with deep trenches and a sphere metalized with thick gold have demonstrated the non-additivity of these forces and the ability to tailor them by suitable surface patterning. Experiments on the Casimir effect in fluids are discussed, including measurements of attractive and repulsive Casimir forces conducted between solids separated by a fluid with $\varepsilon(i\xi)$ intermediate between those of the solids over a large frequency range. Such repulsive forces can be used to achieve quantum levitation in a virtually friction-less environment, a phenomenon that could be exploited in innovative applications to nanomechanics. The last part of the chapter deals with the elusive QED torque between birefringent materials and efforts to observe it. We conclude by highlighting future important directions.

8.1 Introduction

According to QED, quantum fluctuations of the electromagnetic field give rise to a zero-point energy that never vanishes, even in empty space [1]. In 1948, Casimir [2] showed that, as a consequence, two parallel plates, made out of ideal metal (i.e. with unity reflectivity at all wavelengths, or equivalently with infinite plasma frequency), should attract each other in vacuum even if they are electrically neutral, a phenomenon known as the Casimir effect. Because only the electromagnetic modes that have nodes on both walls can exist within the cavity, the zero-point energy depends on the separation between the plates, giving rise to an attractive force. This result in fact can be interpreted as due to the differential radiation pressure associated with zero-point energy (virtual photons) between the "inside" and the "outside" of the plates, which leads to an attraction because the mode density in free space is higher than the density of states between the plates [1]. The interpretation in terms of zero-point energy of the Casimir effect was suggested by Niels Bohr, according to Casimir's autobiography [3]. An equivalent derivation of excellent intuitive value, leading to the Casimir force formula, was recently given by Jaffe and Scardicchio in terms of virtual photons moving along ray optical paths [4, 5]. Between two parallel plates, the Casimir force assumes the form [2]:

$$F_c = -\pi^2 \hbar c A / 240 d^4, \tag{8.1}$$

where c is the speed of light, $\hbar$ is Planck's constant divided by 2π, A is the area of the plates, and d is their separation.

The pioneering experiments of Spaarnay [6] were not able to unambiguously confirm the existence of the Casimir force, due to, among other factors, the large error arising from the difficulty in maintaining a high degree of parallelism between the plates. Clear experimental evidence for the effect was presented by van Blokland and Overbeek in 1978 who performed measurements between a metallic sphere and a metallic plate [7], thus eliminating a major source of

uncertainty. Final decisive verification is due to Lamoureaux, who in 1997 reported the first high precision measurements of the Casimir force using a torsional pendulum and sphere-plate configuration [8]. This was followed by several experimental studies, which have produced further convincing confirmation [9–16] for the Casimir effect including the parallel plate geometry [13].

Between a sphere and a plate made of ideal metals the Casimir force reads [17]:

$$F_c = -\pi^3 \hbar c R/360 d^3, \tag{8.2}$$

where R is the radius of the sphere and d is the minimum distance between the sphere and the plate. In the derivation of (8.2) it was assumed that this distance is much smaller than the sphere diameter (proximity force approximation).

Several reviews on Casimir forces and on the closely related van der Waals forces have recently appeared [18–27]. Both forces are of QED origin. The key physical difference is that in the Casimir case retardation effects due to the finite speed of light cannot be neglected, as in the van der Waals limit, and are actually dominant [1]. This is true for distances such that the propagation time of light between the bodies or two molecules is much greater than the inverse characteristic frequency of the material or of the molecules (for example the inverse plasma frequency in the case of metals and the inverse of the frequency of the dominant transition contributing to the polarizability $\alpha(\omega)$, in the case of molecules) [1]. The complete theory for macroscopic bodies, developed by Lifshitz, Dzyaloshinskii, and Pitaevskii, is valid for any distance between the surfaces and includes in a consistent way both limits [28, 29].

This formulation, a generalization of Casimir's theory to dielectrics, including of course non-ideal metals, is the one which is most often used for comparison with experiments. In this theory, the force between two uncharged surfaces can be derived according to an analytical formula (often called the Lifshitz formula) that relates the zero-point energy to the dielectric functions of the interacting surfaces and of the medium in which they are immersed. This equation for the force between a sphere and plate of the same metal is [28]:

$$F_1(z) = \frac{\hbar}{2\pi c^2} R \int_0^\infty \int_0^\infty p\xi^2 \left\{ \ln\left[1 - \frac{(s-p)^2}{(s+p)^2} e^{-2pz\xi/c}\right] + \ln\left[1 - \frac{(s-p\varepsilon)^2}{(s+p\varepsilon)^2} e^{-2pz\xi/c}\right] \right\} dp d\xi, \tag{8.3}$$

where $s = \sqrt{\varepsilon - 1 + p^2}$, $\varepsilon(i\xi)$ is the dielectric function of the dielectric or metal evaluated at imaginary frequency and the integration is over all frequencies and wavevectors of the modes between the plates. The expression for $\varepsilon(i\xi)$ is given by:

$$\varepsilon(i\xi) = 1 + \frac{2}{\pi} \int_0^\infty \frac{\omega \cdot \varepsilon''(\omega)}{\omega^2 + \xi^2} d\omega, \tag{8.4}$$

where $\varepsilon''(\omega)$ is the imaginary part of the dielectric function. The integral in (8.4) runs over all real frequencies, with non-negligible contributions arising from a very wide range of frequencies. (8.3) and (8.4) show that the optical properties of the material influence in a non-intuitive way the Casimir force. The finite conductivity modifications to the Casimir force based on the frequency dependence of the dielectric function can be calculated numerically using the tabulated complex dielectric function of the metal [30–34]. This leads to a reduction in the Casimir force compared to the ideal metal case given by (8.1). Physically this can be understood from the fact that in a real metal the electromagnetic field penetrates by an amount of the order of the skin-depth which leads to an effective increase of the plate separation. See also the Chap. 10 by van Zwol et al. in this volume for a further discussion of the optical properties of materials used in Casimir force measurements.

The second modification, due to the roughness of the metallic surfaces, tends to increase the attraction [35, 36] because the portions of the surfaces that are locally closer contribute much more to the force due its strong nonlinearity with distance.

As previously mentioned, at very short distances, the theory of Lifshitz, Dzyaloshinskii, and Pitaevskii, also provides a complete description of the non-retarded van der Waals force [37, 38]. Recently Henkel et al. [39] and Intravaia et al. [40] have provided a physically intuitive description of the van der Waals limit for real metals with dispersion described by the Drude model. At finite plasma frequency one must include surface plasmons in the counting of electromagnetic modes, i.e. modes associated with surface charge oscillations which exponentially decay away from the surface. At short distances (small compared to the plasma wavelength) the Casimir energy is given by the shift in the zero-point energy of the surface plasmons due to their Coulomb (electrostatic) interaction. The corresponding attractive force between two parallel plates is then given by [41]:

$$F_c = -\frac{\hbar c \pi^2 A}{290 \lambda_p d^3}. \tag{8.5}$$

This formula is an approximation of the short distance limit of the more complete theory [28, 29]. At large separations ($d \gg \lambda_p$), retardation effects give rise to a long-range interaction that in the case of two ideal metals in vacuum reduces to Casimir's result.

In a number of studies several authors [11, 14, 15] have claimed agreement between Casimir force experiments and theory at the 1% level or better—a claim that has been challenged in some of the literature [12, 42–44]. The authors of [44] have pointed out that the strong non-linear dependence of the force on distance limits the precision in the absolute determination of the force. Uncertainties in the knowledge of the dielectric functions of the thin metallic films used in the experiments and in the models of surface roughness used to correct the Lifshitz theory also typically give rise to errors larger than 1% in the calculation of the expected force [12, 43, 44]. It has also been shown that the calculation of the

Casimir force can vary by as much as 5% depending on which values are chosen for the optical properties of a given material [45]. Another uncertainty is related to the model of surface roughness and in its measurement that translates to an uncertainty in the comparison between theory and experiments. We conclude that claims of agreement between theory and experiment at the 1% level or less are questionable due to experimental errors and uncertainties in the calculations. For a further discussion of modern Casimir force experiments, see the Chap. 7 by Lamoreaux in this volume.

Apart from its intrinsic theoretical interest, the Casimir interaction has recently received considerable attention for its possible technological consequences. The Casimir force, which rapidly increases as the surface separation decreases, is the dominant interaction mechanism between neutral objects at sub-micron distances. In light of the miniaturization process that is moving modern technology towards smaller electromechanical devices, it is reasonable to ask what role the zero-point energy might play in the future development of micro- and nanoelectromechanical systems (MEMS and NEMS) [16, 46, 47].

One of the first experiments was to design a micro-machined torsional device that could be actuated solely by the Casimir force [16]. The results not only demonstrated that this is indeed possible, but also provided one of the most sensitive measurements of the Casimir force between metallized surfaces. In their second experiment [47], the same group showed that the Casimir attraction can also influence the dynamical properties of a micromachined device, changing its resonance frequency, and giving rise to hysteretic behavior and bistability in its frequency response to an ac excitation, as expected for a non-linear oscillator. The authors proposed that this device could serve as a nanometric position sensor. The above developments are covered in Sect. 8.2.

A particularly interesting direction of research on Casimir–Lifshitz forces is the possibility of designing their strength and spatial dependence by suitable control of the boundary conditions of the electromagnetic fields. This can be done by appropriate choice of the materials [48, 49], of the thickness of the metal films [50] and the shape of the interacting surfaces [51–53]. By nanoscale periodic patterning of one of the metallic surfaces and controlling the ratio of the period to the depth of the grooves the Casmir force has been significantly tailored as discussed in Sect. 8.3. This section also discusses experiments aimed at elucidating the role of the skin-depth effect in the Casimir force, by coating one of the surfaces with suitably engineered thin films.

Section 8.3 also covers one of the most interesting features of long-range QED forces: repulsive forces which can arise between suitable surfaces when their dielectric functions and that of the medium separating them satisfy a particular inequality [20, 29, 37, 38]. Measurements of Casimir–Lifshitz forces in fluids are presented, including the measurements of a repulsive force between gold and silicon dioxide separated by bromobenzene. Methods of measuring these forces are discussed in detail and the phenomenon of “quantum levitation” is analyzed along with intriguing applications to nanotechnology such as frictionless bearings and related devices.

QED can give rise to other exotic macroscopic interaction phenomena between materials with anisotropic optical properties such as birefringent crystals. For example a torque due to quantum fluctuations between plates made of uniaxial materials has been predicted but has not yet been observed [54, 55]. Section 8.4 is devoted to discussion of this remarkable effect and related calculations. Specific experiments are proposed along with novel applications.

Section 8.5 provides an outlook on novel directions in this field.

8.2 MEMS Based on the Casimir Force

MEMS are a silicon-based integrated circuit technology with moving mechanical parts that are released by means of etching sacrificial silicon dioxide layers followed by a critical point drying step [56]. They have been finding increasing applications in several areas ranging from actuators and sensors to routers for optical communications. For example the release of the airbag in cars is controlled by a MEMS based accelerometer. In the area of lightwave communications the future will bring about new optical networks with a mesh topology, based on dense wavelength division multiplexing. These intelligent networks will be adaptive and self-healing with capabilities of flexible wavelength provisioning, i.e. the possibility to add and drop wavelengths at specific nodes in response to real time bandwidth demands and rerouting. The *lambda router* [57, 58], a device consisting of an array of thousands of voltage controlled mirrors, which switches an incoming wavelength from one optical fiber to any of many output fibers, is an example of a MEMS technology that might impact future networks.

The development of increasingly complex MEMS will lead to more attention to scaling issues, as this technology evolves towards NanoElecroMechanicalSystems (NEMS). Thus, it is conceivable that a Moore curve for MEMS will develop leading to increasingly complex and compact MEMS having more devices in close proximity [59, 60]. This scenario will inevitably lead to-having to face the issue of Casimir interactions between metallic and dielectric surfaces in close proximity with attention to potentially troublesome phenomena such as stiction, i.e. the irreversible coming into contact of moving parts due to Casimir/van der Waals forces [59]. On the other hand such phenomena might be usable to one's advantage by adding functionality to NEMS based architectures. See also the Chap. 9 by Decca et al. in this volume for additional discussions of MEMS and NEMS based Casimir force experiments.

8.2.1 Actuators

In the first experiment [16], the authors designed and demonstrated a micromachined torsional device that was actuated by the Casimir force and that

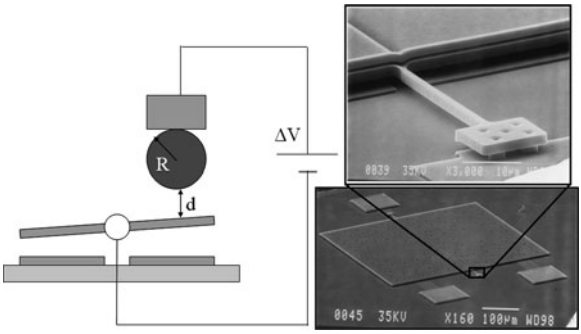

Fig. 8.1 MEMS Casimir force detection setup: schematic of the experiment (not to scale) and scanning electron micrographs of the micromachined torsional device used for the measurement of the Casimir force with a close-up of one of the torsional rods anchored to the substrate. As the metallic sphere approaches the top plate, the Casimir force causes a rotation of the torsional rod

provided a very sensitive measurement of the latter. This device (Fig. 8.1) was subsequently used in a variety of experiments [14, 15, 50, 53]. It consists of a 3.5 μm thick, 500 μm square heavily doped polysilicon plate freely suspended on two of its opposite sides by thin torsional rods. The other ends of the torsional rods are anchored to the substrate via support posts. Two fixed polysilicon electrodes are located symmetrically underneath the plate, one on each side of the torsional rod. Each electrode is half the size of the top plate. There is a 2 μm gap between the top plate and the fixed electrodes created by etching a SiO_2 sacrificial layer. The top plate is thus free to rotate about the torsional rods in response to an external torque.

A schematic of the actuation mechanism based on the Casimir force is shown in Fig. 8.1. A polystyrene sphere with radius $R = 100$ μm is glued on the end of a copper wire using conductive epoxy. A 200 nm thick film of gold with a thin titanium adhesion layer is then evaporated on both the sphere and the top plate of the torsional device. An additional 10 nm of gold is sputtered on the sphere to provide electrical contact to the wire. The micromachined device is placed on a piezoelectric translation stage with the sphere positioned close to one side of the top plate. As the piezo extends, it moves the micromachined device towards the sphere. The rotation of the top plate in response to the attractive Casimir force is detected by measuring the imbalance of the capacitances of the top plate to the two bottom electrodes at different separations between the sphere and the top plate. The measurement is performed at room temperature and at a pressure of less than 1 mTorr. Note that an external bias needs to be applied to the sphere to compensate for the potential V_0 resulting from work function differences between the metallic surfaces and other effects such as contact potentials associated with grounding, patch potential, etc. [7]. The value of V_0 is typically in the 10 to 100 mV range.

Figure 8.2 shows the results of that measurement. One sees that the data points lie above the curve given by (8.2). Two main effects are at work in this

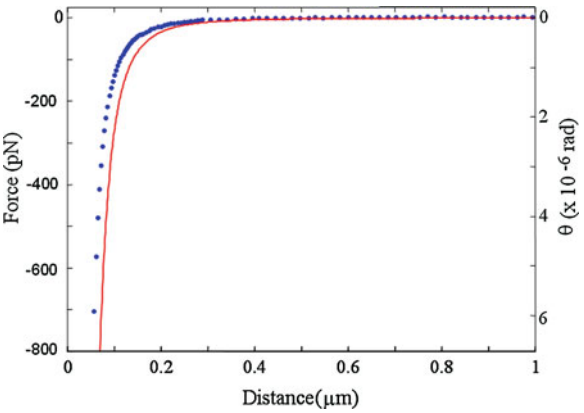

Fig. 8.2 Experimental measurement of the Casimir force from the MEMS torsional apparatus. Angle of rotation of the top plate in response to the Casimir force as a function of distance. The solid line is the predicted Casimir force (8.2) without corrections for surface roughness or finite conductivity. Dots are experimental results

discrepancy. The first one is the finite reflectivity of the metal. This causes virtual photons associated with vacuum fluctuations to penetrate into the metal (skin effect) increasing the effective sphere-plate separation thus decreasing the force. The second effect is the surface roughness, which is estimated from AFM measurements to be a few tens of nanometers depending on the particulars of the experiment. It enhances the Casimir force due to the strong nonlinear dependence with distance. Both effects can be accounted for within the framework of Lifshitz theory, giving a much smaller discrepancy between theory and experiments.

A bridge circuit enables one to measure the change in capacitance to 1 part in 2×10^5, equivalent to a rotation angle of 8×10^{-8} rad, with integration time of 1 s when the device is in vacuum. With a torsional spring constant as small as 1.5×10^{-8} N m rad^{-1}, the device yields a sensitivity of 5 pN Hz$^{-1/2}$ for forces acting at the edge of the plate. Such force sensitivity is comparable to the resolution of conventional atomic force microscopes. The device is insensitive to mechanical noise from the surroundings because the resonant frequency is maintained high enough ($\sim$2 kHz) due to the small moment of inertia of the plate.

8.2.2 Nonlinear Oscillators

While there is vast experimental literature on the hysteretic response and bistability of nonlinear oscillators in the context of quantum optics, solid-state physics, mechanics, and electronics, the experiment summarized in this section represents to our knowledge, the first observation of bistability and hysteresis caused by a QED effect. A simple model of the Casimir oscillator consists of a movable metallic plate subjected to the restoring force of a spring obeying Hooke's law and the nonlinear Casimir force arising from the interaction with a fixed metallic sphere (Fig. 8.3). For separations d larger than a critical value [61], the system is bistable: the potential energy consists of a local minimum and a global minimum

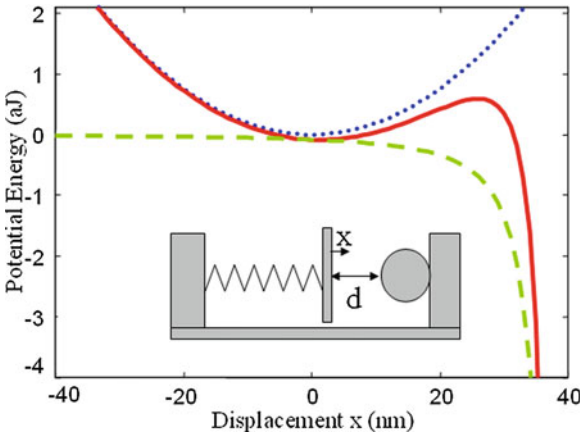

Fig. 8.3 *Inset* a simple model of the nonlinear Casimir oscillator (not to scale). Main figure: elastic potential energy of the spring (*dotted line*, spring constant 0.019 N m^{-1}), energy associated with the Casimir attraction (*dashed line*) and total potential energy (*solid line*) as a function of plate displacement. The distance d between the sphere (100 μm radius) and the equilibrium position of the plate in the absence of the Casimir force, is chosen to be 40 nm

separated by a potential barrier (Fig. 8.3). The local minimum is a stable equilibrium position, about which the plate undergoes small oscillations. The Casimir force modifies the curvature of the confining potential around the minimum, thus changing the natural frequency of oscillation and also introduces higher order terms in the potential, making the oscillations anharmonic.

For this experiment, Fig. 8.1 was used. The torsional mode of oscillation was excited by applying a driving voltage to one of the two electrodes that is fixed in position under the plate. The driving voltage is a small ac excitation V_{ac} with a dc bias V_{dc1} to linearize the voltage dependence of the driving torque. The top plate is grounded while the detection electrode is connected to a dc voltage V_{dc2} through a resistor. Oscillatory motion of the top plate leads to a time varying capacitance between the top plate and the detection electrode. For small oscillations, the change in capacitance is proportional to the rotation of the plate. The detection electrode is connected to an amplifier and a lock-in amplifier measures the output signal at the excitation frequency.

To demonstrate the nonlinear effects introduced by the Casimir force, the piezo was first retracted until the sphere was more than 3.3 μm away from the oscillating plate so that the Casimir force had a negligible effect on the oscillations. The measured frequency response shows a resonance peak that is characteristic of a driven harmonic oscillator (peak I in Fig. 8.4a), regardless of whether the frequency is swept up (hollow squares) or down (solid circles). This ensures that the excitation voltage is small enough so that intrinsic nonlinear effects in the oscillator are negligible in the absence of the Casimir force. The piezo was then extended to bring the sphere close to the top plate while

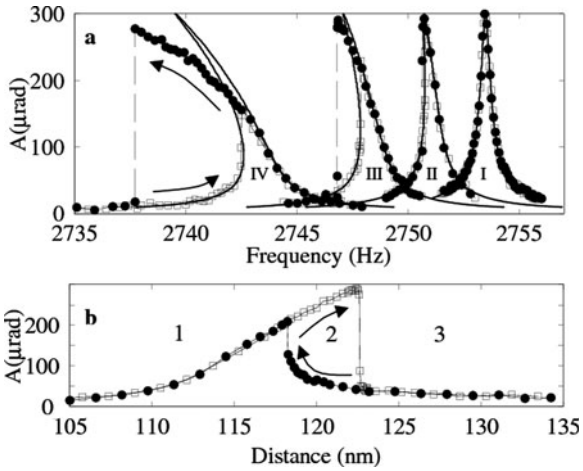

Fig. 8.4 **a** Hysteresis in the frequency response induced by the Casimir force on an otherwise linear oscillator. *Hollow squares* (*solid circles*) are recorded with increasing (decreasing) frequency. *Solid lines* show the predicted frequency response of the oscillator. The distance z between the oscillator and the sphere is 3.3 μm, 141 nm, 116.5 nm, and 98 nm for peaks I, II, III, and IV, respectively. The excitation amplitude is maintained constant at 55.5 mV for all four separations. The solid lines are the calculated response. The peak oscillation amplitude for the plate is 39 nm at its closest point to the sphere. **b** Oscillation amplitude as a function of distance with excitation frequency fixed at 2748 Hz

maintaining the excitation voltage at fixed amplitude. The resonance peak shifts to lower frequencies (peaks II, III, and IV), by an amount that is consistent with the distance dependence of the force in Fig. 8.2. Moreover, the shape of the resonance peak deviates from that of a driven harmonic oscillator and becomes asymmetric. As the distance decreases, the asymmetry becomes stronger and hysteresis occurs. This reproducible hysteretic behavior is characteristic of strongly nonlinear oscillations [62].

The solid lines in Fig. 8.4a show the predicted frequency response of the oscillator including the first, second, and third spatial derivatives of the Casimir force. Higher orders terms or the full nonlinear potential would need to be included to achieve a better agreement with experiments.

An alternative way to demonstrate the "memory" effect of the oscillator is to maintain the excitation at a fixed frequency and vary the distance between the sphere and the plate (Fig. 8.4b). As the distance changes, the resonance frequency of the oscillator shifts, to first order because of the changing force gradient. In region 1, the fixed excitation frequency is higher than the resonance frequency and vice versa for region 3. In region 2, the amplitude of oscillation depends on the history of the plate position. Depending on whether the plate was in region 1 or region 3 before it enters region 2, the amplitude of oscillation differs by up to a factor of 6. This oscillator therefore acts as a nanometric sensor for the separation between two uncharged metallic surfaces.

8.3 The Design and Control of Casimir Forces

In this section we discuss experiments aimed at tailoring the Casimir–Lifshitz force via control of the boundary conditions of the electromagnetic fields. Several examples will be discussed: (1) control of the geometry of the surfaces by nanostructuring with suitable corrugations; (2) control of the thickness of the metallic layers deposited on the juxtaposed surfaces; (3) choice of materials that can be reversibly switched from metallic to transparent and conductive oxides (4) interleaving fluids between the interacting surfaces; (5) material combinations that give rise to repulsive Casimir–Lifshitz force; (6) devices based on repulsive forces.

8.3.1 Modification of the Casimir Force by Surface Nanostructuring

There exists a close connection between the Casimir force between conductors and the van der Waals (vdW) force between molecules (see the chapter of Henkel et al. Chap. 11 in this volume for a discussion of atom-surface effects). For the former, the quantum fluctuations are often associated with the vacuum electromagnetic field, while the latter commonly refers to the interaction between fluctuating dipoles. In simple geometries such as two parallel planes, the Casimir force can be interpreted as an extension of the vdW force in the retarded limit. The interaction between molecules in the two plates is summed to yield the total force. However, such summation of the vdW force is not always valid for extended bodies because the vdW force is not pairwise additive. The interaction between two molecules is affected by the presence of a third molecule. Recently Chan and coworkers [53] reported measurements of the Casimir force between nanostructured silicon surfaces and a gold sphere (Fig. 8.5). One of the interacting objects consists of a silicon surface with nanoscale, high aspect ratio rectangular corrugations. The other surface is a gold-coated glass sphere attached onto a micromechanical torsional oscillator similar to the one discussed in the previous section. Lateral movements of the surfaces are avoided by positioning the corrugations perpendicular to the torsional axis. The Casimir force gradient is measured from the shifts in the resonant frequency of the oscillator at distances between 150 and 500 nm. Deviations of up to 20% from PAA are observed, demonstrating the strong geometry dependence of the Casimir force.

Figure 8.5a shows a cross section of an array of rectangular corrugations with period of 400 nm (sample *B*) fabricated on a highly *p*-doped silicon substrate. Two other samples, one with period 1 μm (sample A) and the other with a flat surface, are also fabricated; the trenches have a depth $t \sim 1$ μm.

The geometry of nanoscale, rectangular trenches was chosen because the Casimir force on such structures is expected to exhibit large deviations from pairwise additive approximation (PAA). Consider the interaction between the

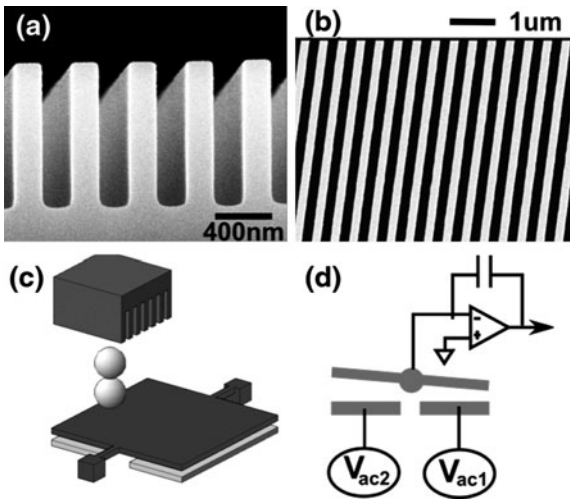

Fig. 8.5 **a** Cross section of rectangular trenches in silicon, with periodicity of 400 nm and depth of 0.98 μm (sample *B*). **b** *Top view* of the structure. **c** Schematic of the experimental setup (not to scale) including the micromechanical torsional oscillator, gold spheres, and silicon trench array. **d** Measurement scheme with electrical connections. Excitation voltages V_{ac1} and V_{ac2} are applied to the bottom electrodes

trench array and a parallel flat surface at distance z from the top surface of the trenches. In the pairwise additive picture, this interaction is a sum of two contributions: the volume from the top surface to the bottom of the trench and the volume below the bottom of the trench. The latter component is negligible because the distance to the other surface is more than 1 μm, larger than the distance range at which Casimir forces can be detected in the experiment. For a trench array of 50% duty cycle, the former component yields exactly half of the interaction between two flat surfaces F_{flat} regardless of the periodicity because half of the material is removed [63]. In practice, the trench arrays are created with duty cycle close to but not exactly at 50%. Under PAA, the total force is equal to pF_{flat}, where p is the fraction of solid volume. The calculation of the Casimir force in such corrugated surfaces, in contrast, is highly nontrivial. While perturbative treatments are valid for smooth profiles with small local curvature, they are impractical for the deep, rectangular corrugations.

Using a different approach based on path integrals, Büscher and Emig [63] calculated the Casimir force for the corrugated geometry made of perfect conductors. Strong deviations from PAA were obtained when the ratio z/λ is large, where λ is the pitch. In the limit when λ goes to zero, the force on a trench array approaches the value between flat surfaces, leading to deviations from PAA by a factor of 2. Such large deviations occur because the Casimir force is associated with confined electromagnetic modes with wavelength comparable to the separation between the interacting objects. When $\lambda \ll z$, these modes fail to penetrate into the trenches, rendering the Casimir force on the corrugated surface equal to a flat one.

For these experiments the gradient of the Casimir force on the silicon trench arrays was measured using a gold-coated sphere attached to a micromechanical torsional oscillator similar to the nonlinear Casmir oscillator previously discussed. The oscillator consists of a 3.5 μm thick, 500 μm square silicon plate suspended

by two torsional rods. As shown in Fig. 8.5c two glass spheres, each with radius R of 50 μm, are stacked and attached by conductive epoxy onto the oscillator at a distance of $b = 210$ μm from the rotation axis. The large distance ($\sim$200 μm) between the oscillator plate and the corrugated surface ensures that the attraction between them is negligible and only the interaction between the top sphere and the corrugated surface is measured. Before attachment, a layer of gold with thickness 400 nm is sputtered onto the spheres. Two electrodes are located between the plate and the substrate. Torsional oscillations in the plate are excited when the voltage on one of the electrodes is modulated at the resonant frequency of the oscillator ($f_0 = 1783$ Hz, quality factor $Q = 32{,}000$). For detecting the oscillations, an additional ac voltage of amplitude 100 mV and frequency of 102 kHz is applied to measure the capacitance change between the top plate and the electrodes. A phase-locked loop is used to track the shifts in the resonance frequency [16, 47] as the sphere approaches the other silicon plate through extension of a closed-loop piezoelectric actuator. As shown in Fig. 8.5c, the movable plate is positioned so that its torsional axis is perpendicular to the trench arrays in the other silicon surface. Such an arrangement eliminates motion of the movable plate in response to possible lateral Casimir forces [64] because the spring constant for translation along the torsional axis is orders of magnitude larger than the orthogonal direction in the plane of the substrate.

The force gradient is measured between the gold sphere and a flat silicon surface [solid circles in Fig. 8.6a] obtained from the same wafer on which the corrugated samples A and B were fabricated. The main source of uncertainty in the measurement ($\sim$0.64 pN μm^{-1} at $z = 300$ nm) originates from the thermomechanical fluctuations of the micromechanical oscillator. As the distance decreases, the oscillation amplitude is reduced to prevent the oscillator from entering the nonlinear regime. At distances below 150 nm, the oscillation amplitude becomes too small for reliable operation of the phase-locked loop. In Fig. 8.6a, the line represents the theoretical force gradient between the gold sphere and the flat silicon surface, including both the finite conductivity and roughness corrections. Lifshiftz's equation is used to take into account the finite conductivity. For the gold surface, tabulated values of the optical properties [32] were used. For the silicon surface, the tabulated values were further modified by the concentration of carriers (2×10^{18} cm^{-3}) determined from the dc conductivity of the wafer (0.028 Ω cm).

Using an atomic force microscope, the main contribution to the roughness was found to originate from the gold surface ($\sim$4 nm rms) rather than the silicon wafer ($\sim$0.6 nm rms), which was taken into account using a geometrical averaging method [65]. The Casimir force gradients $F'_{c;A}$ and $F'_{c;B}$ between the same gold sphere and the corrugated samples A and B were then measured and plotted in Figs. 8.6b and c. As described earlier, under PAA, the forces on the trench arrays (where z is measured from the top of the corrugated surface) are equal to the force on a flat surface multiplied by the fractional volumes p_A and p_B. The solid lines in Fig. 8.6b and c represent the corresponding force gradients, $p_A F'_{c,\mathrm{flat}}$ and $p_B{}' F'_{c,\mathrm{flat}}$, respectively. Measurement of the force gradient was repeated 3 times for each

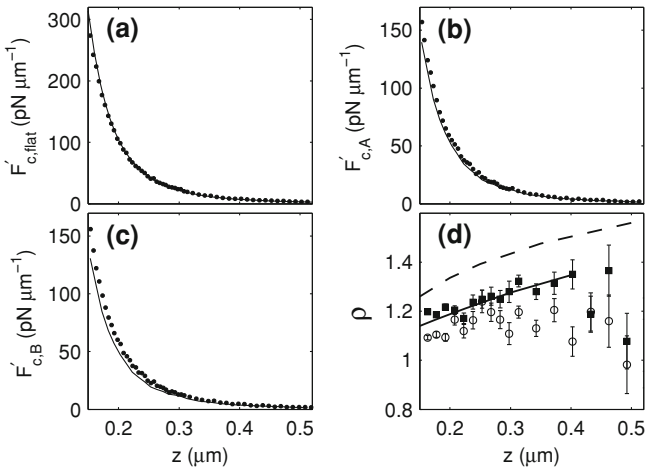

Fig. 8.6 Measured Casimir force gradient between the same gold sphere and **a** a flat silicon surface, $F'_{c,\mathrm{flat}}$, **b** sample A, $F'_{c,A}$ ($\lambda = 1$ μm), and **c** sample B, $F'_{c,B}$ ($\lambda = 400$ nm). In **a**, the *line* represents the theoretical Casimir force gradient including finite conductivity and surface roughness corrections. In **b** and **c**, the *lines* represent the force gradients expected from PAA ($pF'_{c,\mathrm{flat}}$). **d** Ratio ρ of the measured Casimir force gradient to the force gradient expected from PAA, for samples A ($\lambda/a = 1.87$, *hollow circles*) and B ($\lambda/a = 0.82$, *solid squares*), respectively. Theoretical values [63] for perfectly conducting surfaces are plotted as the solid ($\lambda/a = 2$) and dashed lines ($\lambda/a = 1$)

sample, yielding results that are consistent within the measurement uncertainty. To analyze the deviations from PAA, the ratios $\rho_A = F'_{c,A}/p_A F_{c,\mathrm{flat}}$ and $\rho_B = F'_{c,B}/p_B F'_{c,\mathrm{flat}}$ are plotted in Fig. 8.6d. The ratio ρ equals one if PAA is valid. For sample A with $\lambda/a = 1.87$, where a is half the depth of the trenches, the measured force deviates from PAA by $\sim 10\%$. In sample B with $\lambda/a = 0.82$, the deviation increases to $\sim 20\%$. For $150\ \mathrm{nm} < z < 250\ \mathrm{nm}$, the measured Casimir force gradients in both samples show clear deviations from PAA. At larger distances, the uncertainty increases considerably as the force gradient decreases. We compare our experimental results on silicon structures to calculations by Büscher and Emig [63] on perfect conductors [solid and dashed lines in Fig. 8.6d]. In this calculation, the Casimir force between a flat surface and a corrugated structure with $p = 0.5$ was determined for a range of λ/a using a path integral approach. Since $R \gg z$, the proximity force approximation allows a direct comparison of our measured force gradient using a sphere and the predicted force that involved a flat surface. The measured deviation in sample B is larger than sample A, in agreement with the notion that geometry effects become stronger as λ/a decreases. However, the measured deviations from PAA are smaller than the predicted values by about 50%, significantly exceeding the measurement uncertainty for $150\ \mathrm{nm} < z < 250\ \mathrm{nm}$. Such discrepancy is, to a certain extent, expected as a result of the interplay between finite conductivity and geometry effects. The relatively large value of the skin-depth in silicon (~ 11 nm at a wavelength of 300 nm) could

reduce the deviations from PAA. See also the Chap. 4 of Lambrecht et al. in this volume for additional information on material and geometry effects.

8.3.2 Modification of the Casimir Force Between Metallic Films Using the Skin-Depth Effect

The use of ultra-thin metallic coatings (i.e. of thickness comparable to the skin-depth at wavelengths comparable to the distance between the surfaces) over transparent dielectrics, as opposed to thick layers, as employed in the experiments of Sect. 8.2, should alter the distance dependence of the force.

At sub-micron distances, the Casimir force critically depends on the reflectivity of the interacting surfaces for wavelengths in the ultraviolet to far infrared [28, 66]. The attraction between transparent materials is expected to be smaller than that between highly reflective mirrors as a result of a less effective confinement of electromagnetic modes inside the optical cavity defined by the surfaces. A thin metallic film can be transparent to electromagnetic waves that would otherwise be reflected by bulk metal. In fact, when their thickness is much less than the skin-depth, most of the light passes through the film. Consequently, the Casimir force between metallic films should be significantly reduced when its thickness is less than the skin-depth at ultraviolet to infrared wavelengths. For most common metals, this condition is reached when the thickness of the layer is ~ 10 nm.

The technique presented in [66] was recently perfected in terms of the calibration method used and allowed the accurate measurement of the Casimir force for different metal film thickness on the sphere [50].

Demonstrating the skin-depth effect requires careful control of the thickness and surface roughness of the films. The sphere was glued to its support and subsequently coated with a 2.92 nm titanium (Ti) adhesion layer and a 9.23 nm film of palladium (Pd). The thickness of the Ti layer and of the Pd film was measured by Rutherford back scattering [67] on a silicon slice that was evaporated in close proximity to the sphere. After evaporation, the sphere was imaged with an optical profiler to determine its roughness and mounted inside the experimental apparatus. After completion of the Casimir force measurements, the sphere was removed from the experimental apparatus, coated with an additional 200 nm of Pd, analyzed with the optical profiler, and mounted back inside the vacuum chamber for another set of measurements. It is important to stress that the surface roughness measured before and after the deposition of the thicker Pd layer was the same within a few percent.

In Fig. 8.7, the results of the thin film measurements are compared with those obtained after the evaporation of the thick layer of Pd. The measurements were repeated 20 times for both the thin and thick films. The results clearly demonstrate the skin-depth effect on the Casimir force. The force measured with the thin film of Pd is in fact smaller than that observed after the evaporation of the thicker film. Measurements were repeated with a similar sphere: the results confirmed the

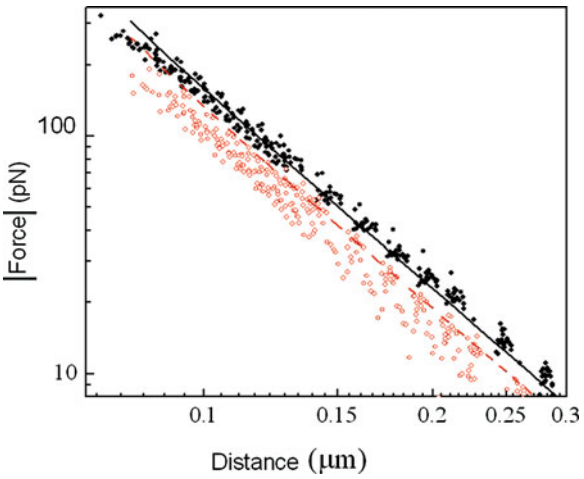

Fig. 8.7 Comparison between Casimir force measurements and calculations for a sphere-plate geometry. *Filled circles* indicate data obtained with a thick metallic film deposited on the plate, while open circles are data for a thin film. Continuous and *dashed lines* represent theoretical predictions for thick and thin films, respectively

skin-depth effect. To rule out possible spurious effects, the data were compared with a theoretical calculation (Fig. 8.7) based on the Lifshitz theory which includes the dielectric function of the metallic coatings and the effects of the surface roughness. The magnitude and spatial distribution of the latter was measured with an optical profilometer and incorporated in the modified Lifshitz equation [36, 50, 68]. The dielectric functions used in the calculation were obtained from Refs. [32–34, 69], and a suitable modification of Lifshitz's theory to account for multiple thin films was used [37].

The discrepancy observed in the case of the thin metallic film is not surprising. The calculation of the force is based on two approximations: (i) the dielectric function for the metallic layers (both titanium and palladium) is assumed to be equal to the one tabulated for bulk-materials, and (ii) the model used to describe the dielectric function of polystyrene is limited to a simplified two-oscillator approximation [69]. These assumptions can lead to significant errors in the estimated force.

8.3.3 Casimir Force Experiments with Transparent Materials

In this section we explore situations in which one of the two noble metal surfaces (typically gold) in Casimir force experiments is replaced by a material that is transparent over a significant range of wavelengths. The expectation would be a large reduction of the Casimir force. Experiments discussed in this section have shown however that to achieve such a reduction the transparency window must be very large. The reason is that, as seen earlier in this chapter, the Casimir–Lifshitz force depends on the dielectric function at imaginary frequencies, which depends on all wavelengths including ones much larger than the plate separation. Here we

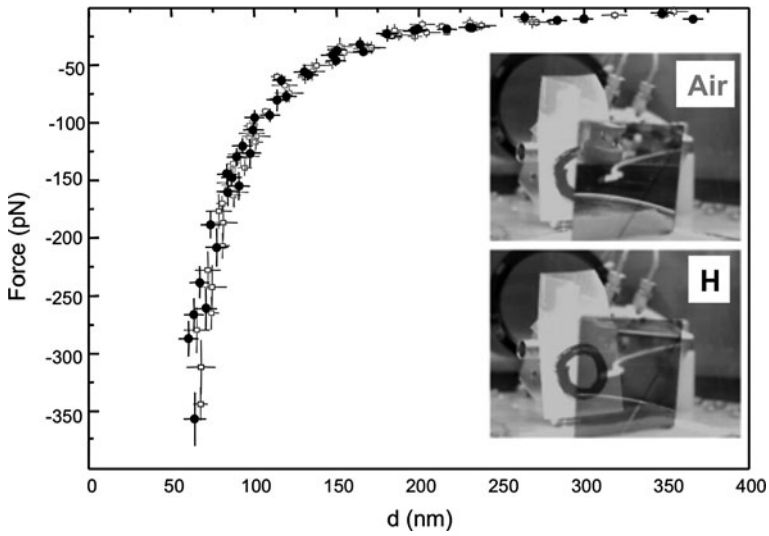

Fig. 8.8 Casimir force between a gold-coated plate and a sphere coated with a Hydrogen Switchable Mirror (HSM) as a function of the distance, in air (*open squares*) and in argon–hydrogen (*filled circles*). *Inset* A HSM in air and in hydrogen. A similar mirror was deposited on the sphere of our experimental apparatus

discuss in detail the case where one of the gold surfaces in the sphere-plate geometry is replaced by a metallic superlattice in which the reflectivity can be tuned by hydrogenation and also include a discussion of a recent experiment in which one of the two surfaces consists of Indium Tin Oxide (ITO), a transparent conductor.

Using the experimental set-up described in Sect. 8.2, the Casimir force between a gold-coated plate and a sphere coated with a Hydrogen Switchable Mirror (HSM) [70] was measured for separations in the 70 to 400 nm range [66]. The HSMs are metallic superlattices obtained by repeating seven consecutive evaporations of alternate layers of magnesium (10 nm) and nickel (2 nm), followed by an evaporation of a thin film of palladium (5 nm). The inset of Fig. 8.8 shows a glass slide coated according to this procedure, both in its as deposited state, and in its hydrogenated state. It is evident that the optical properties of the film are very different in the two situations. The transparency of the film was measured over a wavelength range between 0.5 and 3 μm, and its reflectivity at $\lambda = 660$ nm, keeping the sample in air and in an argon–hydrogen atmosphere (4% hydrogen). The results are in good agreement with the values reported in [71].

The results of Casimir force measurements obtained in air and in a hydrogen-rich atmosphere are shown in Fig. 8.8. It is evident that the force does not change in a discernible way upon hydrogenation of the HSM [66].

In order to explain this apparently surprising result, one should first note that the dielectric properties of the HSMs used in this experiment are known only in a

limited range of wavelengths, spanning approximately the range 0.3–2.5 μm [71]. However, because the separation between the sphere and the plate in the experiment is in the 100 nm range, one could expect that it is not necessary to know the dielectric function for wavelengths longer than 2.5 μm, because those modes should not give rise to large contributions to the force. A mathematical analysis carried out using ad hoc models to describe the interacting surfaces has shown that this is not necessarily the case. Because the Casimir force depends on the dielectric function at imaginary frequency (8.4) and the integral in the latter is over all frequencies, long wavelengths compared to the separation between the sphere and the plate can make a significant contribution to the force. Thus, one of the reasons for not having observed a change in the latter upon hydrogenation is likely related to the fact that that the imaginary part of the permittivity might not change significantly at long wavelengths. Recently, a more accurate analysis of the experiment [72] confirmed this result, but also added an important detail: for a correct comparison of data with theory it is necessary take into account also the presence of the 5 nm thick palladium layer that was deposited on top of the HSMs to prevent oxidation and promote hydrogen absorption. Although this layer is fairly transparent to all wavelengths from ultraviolet to infrared, its contribution to the interaction reduces the expected change of the force by nearly a factor of two. It is thus the combination of the effect of the reflectivity at long wavelengths and of the thin palladium film that limits the magnitude of the change of the force following hydrogenation. Still, calculations show that a small change in the Casimir force upon hydrogenation should be observable with improved experimental precision and with the use of HSMs of different composition [72].

Recently the group of Davide Iannuzzi reported a precise measurement in air of the Casimir force between a gold-coated sphere and a glass plate coated with either a thick gold layer or a highly conductive, transparent ITO film [73]. The decrease of the Casimir force due to the different dielectric properties of the reflective gold layer and the transparent oxide film resulted to be as high as 40%–50% at all separations (from 50 to 150 nm). Physically the large reduction of the Casimir force when the Au surface is replaced by ITO is due to the much smaller plasma frequency of ITO (in the near infrared spectrum) compared to that of Au (in the ultraviolet). This experiment shows that, in the presence of a conductive oxide layer, the Casimir force can still be the dominant interaction mechanism even in air, and indicates that, whenever the design might require it, it is possible to tune the Casimir attraction by a factor of 2.

8.3.4 Casimir Forces in a Fluid

To measure the Casimir force in a fluid, a modified atomic force microscopy (AFM) method can be used as shown in Fig. 8.9 [74, 75]. Light from a superluminescent diode is reflected off the back of the cantilever and is detected by a four-quadrant photodetector, which is used to monitor the deflection of the

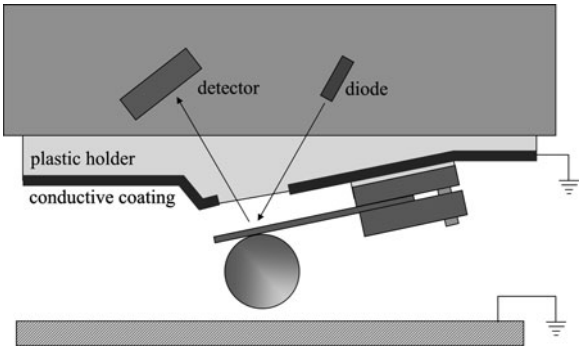

Fig. 8.9 Experimental setup. A polystyrene sphere is attached to an AFM cantilever and coated with gold. A laser beam is directed through a few millimeter opening in the conductive coating of the cantilever holder and is reflected off the back of the cantilever to monitor its motion

cantilever, as in standard AFM measurements. The difference signal between the top two quadrants and the bottom two quadrants is proportional to the vertical deflection of the cantilever. A piezoelectric column within the AFM is used to advance the cantilever and sphere toward the plate, and the piezoelectric column's advance is detected using a linear variable differential transformer, which minimizes nonlinearities and hysteresis inherent in piezoelectrics. As the sphere approaches the plate, any force between the two will result in a deflection of the cantilever, which will then be detected in the difference signal from the four-quadrant detector. Cleaning and calibration techniques can be used to isolate the Casimir force from other spurious forces (e.g. electrostatic and hydrodynamic) and to convert the deflection signal into a force signal [74–76].

Figure 8.10 shows the Casimir–Lifshitz force in ethanol between the gold-coated sphere and gold-coated plate. The data for 51 runs are shown (dots) along with the average of these data (circles) and Lifshitz theory for ethanol separating the two surfaces and no added salt (solid line). The theory describes the data well, despite the uncertainties in the optical properties. Deviations between the theory and experiment below 30 nm are likely due to the inability of the theory to accurately describe the surface roughness on these scales and the uncertainty in the optical properties.

The Casimir–Lifshitz force for different salt concentrations is shown in Fig. 8.10b along with Lifshitz's theory without corrections due to electrostatics or zero-frequency screening [75]. The data is shown for experiments with no added salt (circles), 0.3 mM NaI (squares), and 30 mM NaI (triangles) and is obtained by averaging 51 data set for each concentration. The inset shows a log–log plot of the data. The difference between the forces due to the modification of the zero-frequency contribution and the Debye screening are greater for smaller separations and both are calculated to be ~ 15 pN in the range from 30–40 nm; however, the sensitivity of our apparatus is not adequate to distinguish a significant difference between these curves. Further experimental details can be found in Ref. [75].

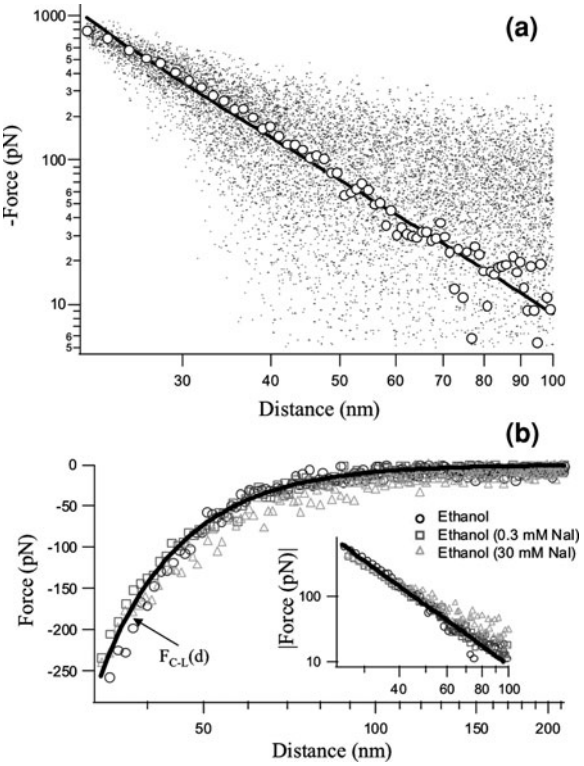

Fig. 8.10 **a** Measured force between a gold sphere and a gold plate immersed in liquid ethanol is well described by Lifshitz's theory. Dots represent measurements from 51 runs. Circles are average values from the 51 data sets. Solid line is Lifshitz's theory. **b** Comparison of the measured force with different concentrations of salt shows no significant difference. Force data in ethanol with no added salt (*circles*), 0.3 mM NaI (*squares*), and 30 mM NaI (*triangles*). Lifshitz's theory for no added salt is shown as a *solid line*. *Inset* log–log plot of the data

8.3.5 Repulsive Forces and Casimir Levitation

Modification of the Casimir force is of great interest from both a fundamental and an applied point-of-view. It is reasonable to ask whether such modifications can lead to repulsive forces in special cases. In 1968, T.H. Boyer showed that for a perfectly conducting spherical shell the Casimir effect should give rise to an outward pressure [77]. Similar repulsive Casimir forces have also been predicted for cubic and rectangular cavities with specific aspect ratios [78, 79]. However, criticisms concerning these results have been raised [80], and recently the possibility of repulsive forces based on topology for a wide class of systems has been ruled out [81].

The possibility of topological repulsive Casimir forces, i.e. due to the geometrical structure of the interacting metallic bodies in vacuum, is therefore controversial. In this section, we will describe a repulsive force that is due strictly to the optical properties of the materials involved. Such a mechanism is responsible for many phenomena in the non-retarded regime including the surface melting of solids [82] and the vertical ascent of liquid helium within a container (see, for example, the discussion in Refs. [20, 29, 83]).

As was demonstrated by Dzyaloshinskii, Lifshitz, and Pitaevskii in their seminal paper, the sign of the force depends on the dielectric properties of materials involved [29]. See also the Chap. 2 by Pitaevskii in this volume for related discussions. Two plates made out of the same material will always attract, regardless of the choice of the intermediate material (typically a fluid or vacuum); however, between slabs of different materials (here labeled 1 and 2) the force becomes repulsive by suitably choosing the intermediate liquid (labeled 3). Thus, by proper choice of materials, the Casimir–Lifshitz force between slabs 1 and 2 can be either attractive or repulsive. Specifically, the condition for repulsion is:

$$\varepsilon_1 > \varepsilon_3 > \varepsilon_2, \tag{8.6}$$

Here the dielectric functions $\varepsilon_1, \varepsilon_2$ and ε_3, of the materials are evaluated at imaginary frequencies. Because they vary with frequency, it is conceivable that inequality (8.6) may be satisfied for some frequencies and not for others. For various separations between the slabs, different frequencies will contribute with different strengths, which can lead to a change in the sign of the force as a function of separation.

In order to qualitatively understand the origin of these repulsive forces, we consider the following toy model (see Fig. 8.11 and Ref. [84]) for the microscopic interaction of the bodies. To first order, the force between the latter is dominated by the pair-wise summation of the van der Waals forces between all the constituent molecules. This additivity is a good approximation for rarefied media; however, the force between two molecules is affected in general by the presence of a third. Hamaker first used this approach in extending the calculations of London to the short-range interaction (i.e. the non-retarded van der Waals force) between bodies and in particular to those immersed in a fluid. By suitably choosing three materials and their constituent molecules so that their polarizabilities satisfy the inequality $\alpha_1 > \alpha_3 > \alpha_2$, we find the forces between the individual molecules, which are proportional to the product of the polarizabilites integrated over all imaginary frequencies, will obey: $F_{13} > F_{12} > F_{23}$, where the subscript ij represents the interaction between molecules i and j. Thus, it is energetically more favorable for molecule 3 to be near molecule 1 than it is for molecule 2 to be near molecule 1. As more molecules of the same species are added to the system, molecules of type 3 will be strongly attracted to those of type 1, resulting in an increased separation for molecules of type 2 from those of type 1. In this way, Hamaker showed that repulsive forces between two different materials immersed in a liquid are possible by calculating the total interaction energy between the bodies and the fluid as the separation between the bodies is varied. His calculations however were non-rigorous because they neglected non-additivity and retardation effects. When these are included, long-range repulsion between two bodies (materials 1 and 2) separated by a third (material 3) is predicted when their relative dielectric functions obey (8.6). Note that when the fluid has the largest dielectric function, the cohesive van der Waals interaction within the fluid results in an attraction between its molecules that is larger than that between the molecules of the fluid and the plate, which leads to an attractive force between the two plates.

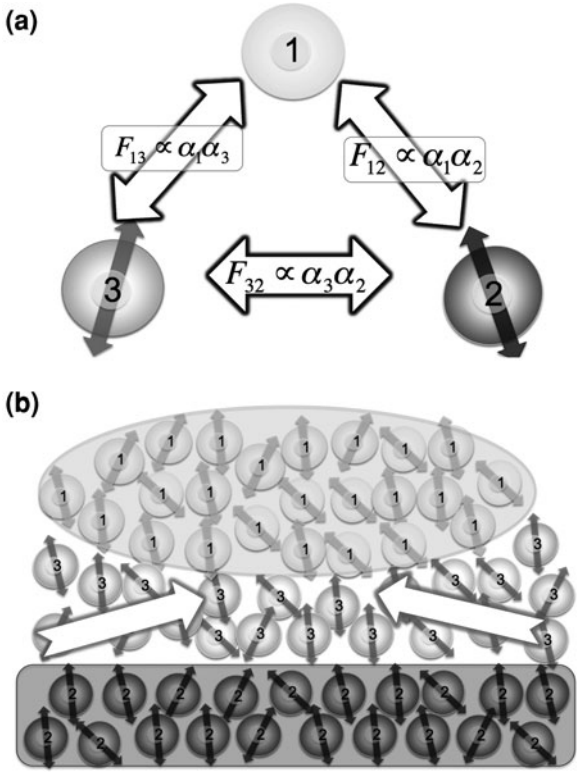

Fig. 8.11 Toy model of repulsive Casimir–Lifshitz forces. Repulsive forces can exist between two materials, schematically represented as an ensemble of molecules separated by a third, typically a liquid, with specific optical properties. **a** Three individual molecules will all experience attractive interactions. **b** For a collection of molecules, with $\alpha_1 > \alpha_3 > \alpha_2$, it is energetically more favorable for the molecules with the largest polarizabilities (α_1 and α_3 for this example) to be close, resulting in an increased separation between molecules of type 1 and type 2. For a condensed system, the net interaction between material 1 and material 2 is repulsive if the corresponding dielectric functions satisfy $\varepsilon_1 > \varepsilon_3 > \varepsilon_2$, as consequence of the similar inequality between polarizabilities. Note that all the α's and the ε's need to be evaluated at imaginary frequencies (see text)

Examples of material systems that obey (8.6) are rare but do exist. One of the earliest triumphs of Lifshitz's equation was the quantitative explanation of the thickening of a superfluid helium film on the walls of a container [29, 83]. In that system, it is energetically more favourable for the liquid to be between the vapour and the container, and the liquid climbs the wall. One set of materials (solid–liquid–solid) that obeys inequality (8.6) over a large frequency range is gold, bromobenzene, and silica (Fig. 8.12).

Using the above-mentioned material combination, we have shown that repulsive Casimir–Lifshitz forces are measureable [76]. Raw deflection versus piezo

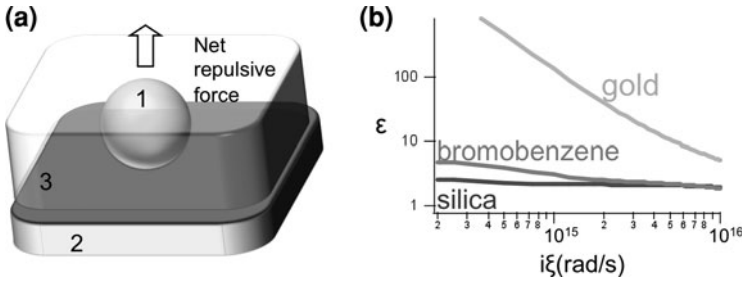

Fig. 8.12 Repulsive quantum electrodynamical forces can exist for two materials separated by a fluid. **a** The interaction between material *1* and material *2* immersed in a fluid (material *3*) is repulsive when $\varepsilon_1(i\xi) > \varepsilon_3(i\xi) > \varepsilon_2(i\xi)$, where the $\varepsilon(i\xi)$'s are the dielectric functions at imaginary frequency. **b** The optical properties of gold, bromobenzene, and silica are such that $\varepsilon_{\text{gold}}(i\xi) > \varepsilon_{\text{bromobenzene}}(i\xi) > \varepsilon_{\text{silica}}(i\xi)$ and lead to a repulsive force between the gold and silica surfaces

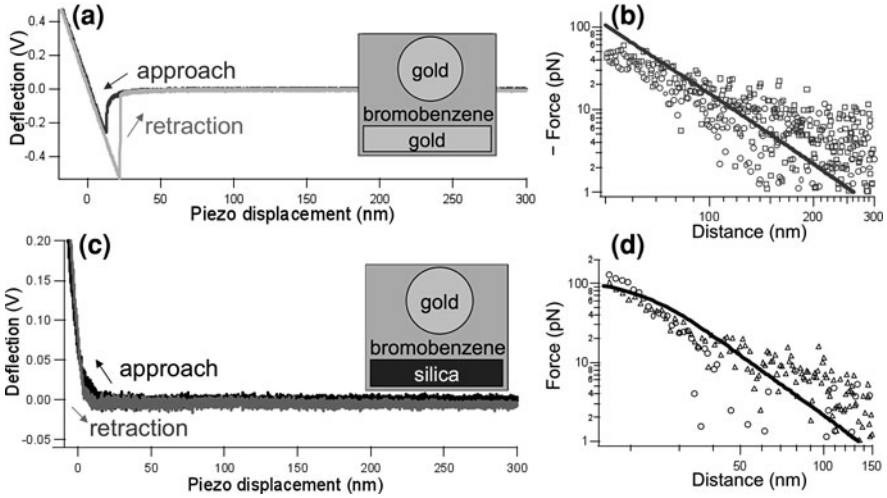

Fig. 8.13 Attractive and repulsive Casimir–Lifshitz force measurements. **a** Deflection data showing attractive interactions between a gold sphere and a gold plate. **c** For the case of the same gold sphere and a silica plate, deflection data show a repulsive interaction evident during both approach and retraction. **d** Measured repulsive force between a gold sphere and a silica plate on a log–log scale (*circles*) and calculated force using Lifshitz's theory (*solid line*) including corrections for the measured surface roughness of the sphere and the plate. Triangles are force data for another gold sphere (nominally of the same diameter)/silica plate pair. **b** Measured attractive force on a log–log scale for two gold sphere/plate pairs (*circles* and *squares*) and calculated force using Lifshitz's theory (*solid line*) including surface roughness corrections corresponding to the data represented by the circles

displacement data show that the force is changed from attractive to repulsive by replacing the gold plate with the silica plate [Fig. 8.13a,c]. The data in Fig. 8.13a,c were acquired with a piezo speed of 45 nm/s. With the gold plate,

the cantilever is bent toward the surface during the approach, which corresponds to an attractive force between the sphere and plate until contact [Fig. 8.13a]. Once contact is made, the normal force of the plate pushes against the sphere. Upon retraction, the sphere sticks to the plate for an additional 10 nm, due to stiction between the two gold surfaces, before losing contact with the surface. When the silica plate is used, the cantilever is bent away from the surface during the approach, corresponding to a repulsive interaction [Fig. 8.13c]. During retraction, the sphere continues to show repulsion. This cannot be a result of the hydrodynamic force, because the hydrodynamic force is in a direction that opposes the motion of the sphere and will change sign as the direction is changed. Similarly, the repulsion observed in Fig. 8.13c cannot be due to charge trapped on silica; any charge that does exist on the surface will induce an image charge of opposite sign on the metal sphere and lead to an attractive interaction. Further experimental details can be found in Ref. [76], and a critical analysis of previous experiments in the van der Waals regime are discussed in Ref. [84] and briefly at the end of this section.

The measured forces after calibration show a clear distinction between the attractive and repulsive regimes when the plate is changed from gold to silica (Fig. 8.13b,d). The circles correspond to the average force from 50 runs between the gold sphere and the plate. Histograms of the force data at different distances show a Gaussian distribution and no evidence of systematic errors.

The experiment is repeated with an additional sphere and plate for both configurations. Figure 8.13b shows the measured force for two different spheres of nominally the same diameter and two different gold plates. Similar measurements for two spheres and silica plates are shown in Fig. 8.13d. The solid lines are the temperature dependent Lifshitz's theory including surface roughness corrections for the first sphere/plate pair (circles). Because the second set of measurements are made with spheres and plates of similar surface roughness and size, the corrections are of similar magnitude.

Prior to our work, previous experiments have shown evidence for short-range repulsive forces in the van der Waals regime [85–90]; however, there are many experimental issues that must be considered that, as our analysis below shows, were not adequately addressed in many of these experiments. For separations of a few nm or less, liquid orientation, solvation, and hydration forces become important and should be considered, which are not an issue at larger separations. Surface charging effects are important for all distance ranges. In order to satisfy (8.6), one of the solid materials must have a dielectric function that is lower than the dielectric function of the intermediate fluid. One common choice for this solid material is PTFE (polytetrafluoroethylene), which was used in most experiments [86, 88–90]; however, as was pointed out in Ref. [86], residual carboxyl groups and other impurities can easily be transferred from the PTFE to the other surface, which complicates the detection and isolation of the van der Waals force. In a few experiments, the sign of the force did not agree with the theoretical calculation, which may be attributed to additional electrostatic force contributions [85, 86]. To avoid this problem, Meurk et al.

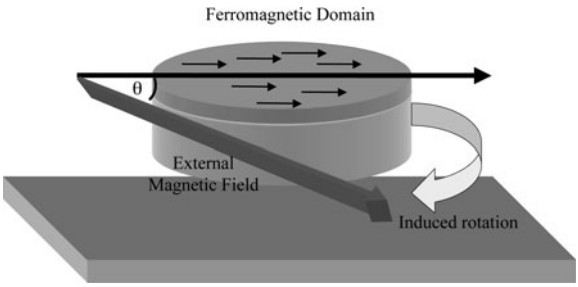

Fig. 8.14 QED levitation device. A repulsive force develops between the disk immersed in a fluid and the plate, which is balanced by gravity. We show a nano-compass that could be developed to mechanically sense small magnetic fields

performed experiments with inorganic samples [87]; however, the experimental configuration consisted of a sharp tip and a plate, which limited the surface separations to below 2 nm. For the determination of the cantilever force constant, either the Sader method [91] or the Cleveland method [92] was used in these experiments. The Sader method gives the spring constant of a cantilever based on the geometry of the cantilever and its resonance frequency, and the Cleveland method uses the resonance frequency shift of a cantilever upon the addition of masses to determine the spring constant. These methods lead to an additional 10–20% error in the determination of the force [93], which could be greatly reduced if a calibration method is performed that uses a known force for the calibration [74, 75, 94]. Finally, the determination of the absolute distance was often found by performing a fit of the experimental data to the presumed power law of the van der Waals force [86, 88–90]. Thus, the absolute surface separation could only be determined if one assumed that the measured force was only the van der Waals force and that it was described precisely by a $1/d^2$ force law.

8.3.6 Devices Based on Repulsive Casimir Forces

Repulsive Casimir–Lifshitz forces could be of significant interest technologically as this technique might be used to develop ultra-sensitive force and torque sensors by counterbalancing gravity to levitate an object immersed in fluid above a surface without disturbing electric or magnetic interactions. Because the surfaces never come into direct contact as a result of their mutual repulsion, these objects are free to rotate or translate relative to each other with virtually no static friction. Dynamical damping due to viscosity will put limits on how quickly such a device can respond to changes in its surroundings; however, in principle even the smallest translations or rotations can be detected on longer time scales. Thus, force and torque sensors could be developed that surpass those currently used. Figure 8.14 shows an example of a QED levitation device: a nano-compass sensitive to very small static magnetic fields [95].

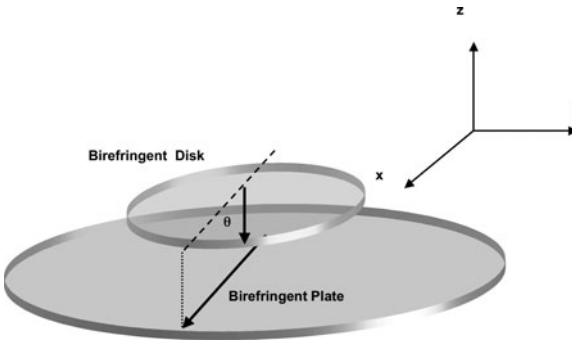

Fig. 8.15 A QED torque develops between two birefringent parallel plates with in-plane optical axis when they are placed in close proximity

8.4 QED Torque

The effect of the zero-point energy between two optically anisotropic materials, as shown in Fig. 8.15, has also been considered [54, 55, 95, 97–103]. In this case, the fluctuating electromagnetic fields have boundary conditions that depend on the relative orientation of the optical axes of the materials; hence, the zero-point energy arising from these fields also has an angular dependence. This leads to a torque that tends to align two of the principal axes of the materials in order to minimize the system's energy. We have recently shown that such torques should indeed be measurable and have suggested experimental configurations to perform these measurements [102, 103].

In 1972 Parsegian and Weiss derived an expression for the short-range, non-retarded van der Waals interaction energy between two semi-infinite dielectrically anisotropic materials immersed within a third material [54]. This result, obtained by the summation of the electromagnetic surface mode fluctuations, showed that the interaction energy was inversely proportional to the separation squared and depended on the angle between the optical axes of the two anisotropic materials. In 1978, Barash independently derived an expression for the interaction energy between two anisotropic materials using the Helmholtz free energy of the electromagnetic modes, which included retardation effects [55]. In the non-retarded limit, Barash's expression confirmed the inverse square distance dependence of Parsegian and Weiss and that the torque, in this limit, varies as $\sin(2\theta)$, where θ is the angle between the optical axes of the materials.

The equations that govern the torque in the general case of arbitrary distances are quite cumbersome and are treated in detail elsewhere [55, 102]. For brevity, we refer the reader to those papers for a more in-depth analysis and simply state a few of the relevant results. First, the torque is proportional to the surface area of the interacting materials and decreases with increasing surface separation. Second it is found that the QED torque at a given distance varies as:

$$M = A \sin(2\theta), \tag{8.7}$$

even in the retarded limit, where A is the value of the torque at $\theta = \pi/4$. Figure 8.16a shows the torque as a function of angle for a 40 μm diameter calcite disk in vacuum above a barium titanate plate at a distance of $d = 100$ nm [102]. The circles correspond to the calculated values of the torque, while the solid line corresponds to a best fit with (8.7).

Experimentally it is difficult to use large disks in close proximity, because at such small separations tolerances in the parallelism of two large surfaces (tens of microns in diameter) are extremely tight; in addition it is difficult to keep them free of dust and contaminants. If the vacuum is replaced by liquid ethanol, the torque remains of the same order of magnitude; however, the three materials (calcite, ethanol, and barium titanate) have dielectric functions that obey (8.6). This will result in a repulsive Casimir–Lifshitz force which will counterbalance the weight of the disk and allow it to float at a predetermined distance above the plate. For a 20 μm thick calcite disk with a diameter of 40 μm above a barium titanate plate in ethanol, the equilibrium separation was calculated to be approximately 100 nm with a maximum torque of $\sim 4 \times 10^{-19}$ N m [102], as shown in Fig. 8.16b.

For the observation of the QED torque, it was suggested in [102] that the disk be rotated by $\theta = \pi/4$ by means of the transfer of angular momentum of light from a polarized beam. The laser could then be shuttered, and one would visually observe the rotation of the disk back to its minimum energy orientation. The amount of angular momentum transfer determines the initial value of the angle of rotation. After the laser beam is blocked the disk can rotate either clockwise or counterclockwise back to the equilibrium position depending on the value of the initial angle, making it possible to verify the $\sin(2\theta)$ dependence of the torque. Procedures to minimize the effect of charges on the plates and other artifacts were also discussed [102].

An alternative scheme involving the statistical analysis of Brownian motion was recently described in [103]. For this situation, the disk size is reduced to the point that Brownian motion causes translation and rotation. When these rotations become comparable to the QED rotation, the disk will no longer rotate smoothly to its minimum energy configuration. Instead the angle between the optical axes will fluctuate to sample all angles. The probability distribution for the observation of the angle θ between the two optical axes is:

$$p(\theta) = p_o \exp[-U(\theta)/k_B T], \tag{8.8}$$

where $U(\theta)$ is the potential energy of the QED orientation interaction, i.e. the energy associated with the torque, $k_B T$ is the thermal energy, p_o is a normalization constant such that $\int p(\theta)\, d\theta = 1$. By observing the angle between the axes as a function of time, one can deduce the probability distribution via a histogram of the angular orientations as shown in Fig. 8.17. This is similar to the determination of the potential energy as a function of distance in Total Internal Reflection Microscopy (TIRM) experiments for optically trapped spherical particles [104, 105].

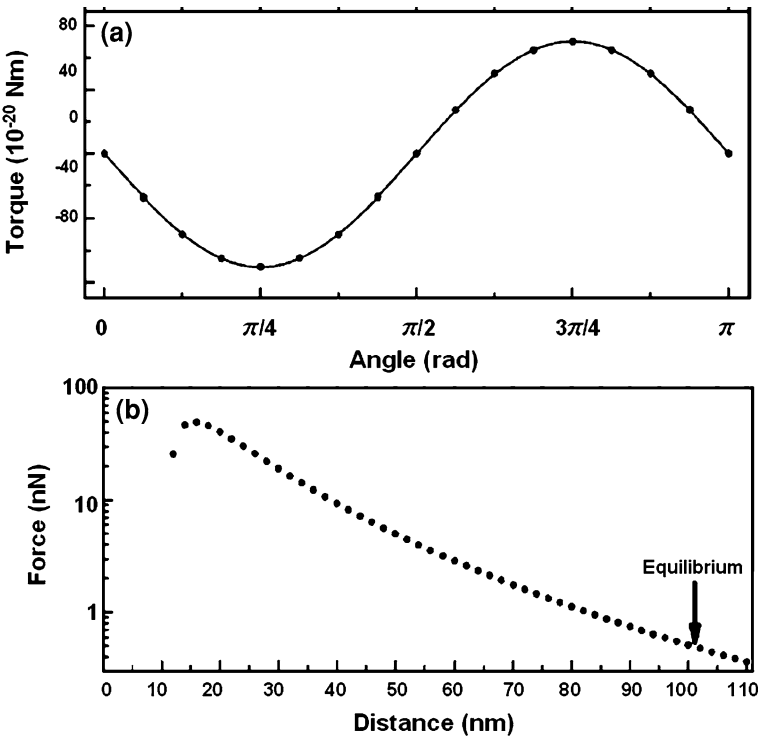

Fig. 8.16 **a** Calculated torque as a function of angle between a 40 μm diameter disk made of calcite and a barium titanate plate separated in vacuum by a distance $d = 100$ nm. The *lines* represent a fit (8.7). **b** Calculated retarded van der Waals force as a function of plate separation for this system at a rotation angle of $\pi/4$. The *arrow* represents the distance at which the retarded van der Waals repulsion is in equilibrium with the weight of the disk

To observe this effect, one needs to levitate a birefringent disk above a birefringent plate at short-range and be able to detect the orientation of the axes. This can be done either by using a repulsive Casimir–Lifshitz force or a double layer repulsion force [38] and video microscopy techniques [106] as described below.

The equilibrium separation occurs when the sum of the forces (Casimir–Lifshitz, double layer, and weight) acting on the particle is zero:

$$\sum F = F_{CL}(d) + D \times \exp[-d/l] - \pi R^2 h \Delta\rho g = 0, \tag{8.9}$$

where $F_{CL}(d)$ is the Casimir–Lifshitz force at distance d, D is a constant related to the Poisson-Boltzmann potential evaluated at the surface due to charging, l is the Debye length, R is the radius of the disk, h is the thickness of the disk, $\Delta\rho$ is the density difference between the disk and the solution, and g is the acceleration due to gravity. Both the Casimir–Lifshitz force and the weight of the disks are set by the geometry of the system and the materials chosen; however, the double layer force

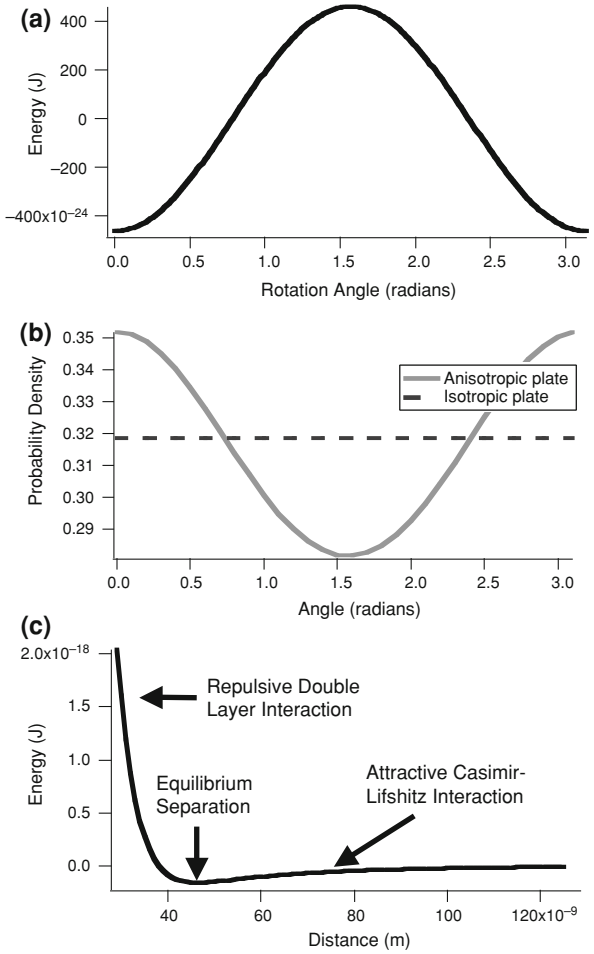

Fig. 8.17 QED interaction energies and probabilities. **a** Calculations of the angular dependence of the QED interaction energy between a 2 lm diameter LiNbO3 disk and a calcite plate. **b** Probability of detecting a rotation θ. **c** Energy as a function of separation between the disk and plate including contributions from the double layer interaction (dominant at close range), the Casimir–Lifshitz interaction (dominant at longer range) and gravity (negligible). Equilibrium is obtained around 50 nm

can be modified by changing the electrolyte concentration. Thus, the floatation height can be adjusted in this way. Figure 8.17c shows the approximate interaction energy following from the forces of (8.9), where we have chosen a double layer interaction leading to a levitation height of approximately 50 nm, with deviations of a few nm due to thermal energy (k_BT), for a lithium niobate disk with radius $R = 1$ μm and thickness $h = 0.5$ μm in an aqueous solution above a calcite plate.

In order to track the motion of the disk above the plate, a video microscopy setup similar to the one described in [106] is used. The disk's motion is tracked and

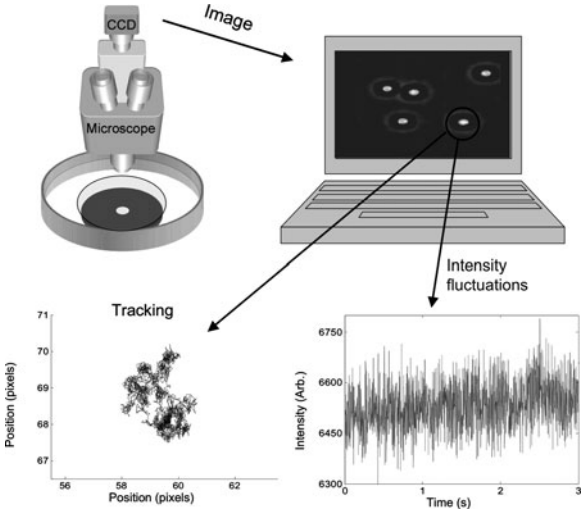

Fig. 8.18 Schematic of the Brownian motion detection scheme showing data for a non-birefringent spherical particle. Light is recorded via a CCD and digitized to allow for tracking and determination of intensity fluctuations

recorded as is the intensity of the transmitted light. The orientation of the disk is determined by placing it between a combination of polarizing optical components so that the intensity of the transmitted light can be related to the orientation of the optical axis. In order to determine the expected optical intensity at the output as a function of θ, the Jones matrix representation of the optical elements is used to determine the exiting E-field from which the intensity is calculated [107, 108]. For suitably chosen optical components (see Ref. [103]), the intensity is proportional to $[1 - \cos(2\theta)]$. From histogram of the intensities, we can determine the preferred angular orientation of the disk and hence the angular QED interaction energy and the torque.

Figure 8.18 shows the typical configuration for such experiments. The thermal fluctuations of the particles are recorded via a CCD camera attached to an upright microscope. The particles' centers can be determined and tracked by the method of [106] with a standard deviation of less than 1/10 pixel. Figure 8.18 shows both the tracking and intensity fluctuations recorded for a spherical non-birefringent particle. For non-birefringent particles, the intensity fluctuations are due to scattering by the particle as it undergoes Brownian motion. In order to study the QED torque, small birefringent disks should be used. Such disks have been fabricated using a combination of crystal ion slicing [109], mechanical polishing, and focused ion beam (FIB) sculpting as shown in Fig. 8.19. To date no experiments have been performed with birefringent particles; however, this detection scheme should be suitable for such QED torque experiments.

8.5 Future Directions

A number of other interesting QED phenomena await experimental investigation:

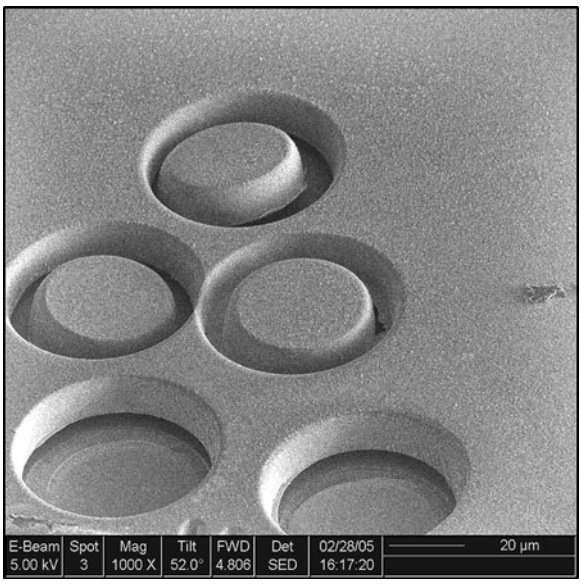

Fig. 8.19 LiNbO3 disks fabricated by crystal ion slicing and focused ion beam sculpting

8.5.1 Phase Transitions and the Casimir Effect

Recently the influence of Casimir energy on the critical field of a superconducting film has been theoretically investigated, and it was shown that it might be possible to directly measure the variation of Casimir energy that accompanies the superconducting transition [110]. Another interesting experiment would be to use as one of the surfaces a vanadium oxide film. This material switches from insulator to metal above a temperature of ~ 60 C and such a transition with the attendant significant change in reflectivity is expected to lead to an observable increase of the Casimir force above that temperature. Recent measurements on another material (Ag-In-Sb-Te) that can undergo a phase transition has shown a modification of the Casimir force by up to 20% when samples prepared from either crystalline or amorphous phases were used [111].

8.5.2 Self Assembly and Sorting via the Casimir–Lifshitz Force

The ability to modify the Casimir–Lifshitz force opens the door to the possibility of engineering the potential energy landscape for particles based purely on their dielectric functions [84]. With the appropriate choice of fluid, repulsive forces will occur for asymmetric configurations (e.g. Au-SiO_2 across bromobenzene), while attractive forces will occur for symmetric configurations (e.g. Au-Au or SiO_2-SiO_2 across bromobenzene). By patterning a plate with these two different materials,

one can study both non-additivity effects discussed above and the assembly and sorting of particles based solely on their dielectric functions. Similar sorting and aggregation effects have been observed in the thermodynamic Casimir effect, which is related to classical density fluctuations [112]. Other recent proposals include the ability to tune chemical reactions [113] and the self-assembly of colloidal scale devices [114, 115] based, at least partially, on manipulating the Casimir–Lifshitz forces.

8.5.3 Casimir Friction

There has been an interesting prediction that dissipative retarded van der Waals forces can arise between surfaces in relative motion due to the exchange of virtual photons which couple to acoustic phonons in the material [116]. Similar dissipative Casimir forces can arise between metals; here virtual photons would couple to particle-hole excitations in the metal [117]. This would lead to changes with position of the Q of suitable MEMS oscillators, such as the ones described in Sect. 8.2.2.

J. B. Pendry has considered another type of vacuum friction when two perfectly smooth featureless surfaces at $T = 0$, defined only by their respective dielectric functions, separated by a finite distance, move parallel to each other [118]. He found large frictional effects comparable to everyday frictional forces provided that the materials have resistivities of the order of 1 MΩ and that the surfaces are in close proximity. The friction depends solely on the reflection coefficients of the surfaces for electromagnetic waves, and its detailed behavior with shear velocity and separation is controlled by the dispersion of the reflectivity with frequency. There exists a potentially rich variety of vacuum friction effects, as discussed in a recent article [119]. See also the discussion in the Chap. 13 of Dalvit et al. and Henkel et al. Chap. 11 of this volume.

8.5.4 Dynamic Casimir Effect

It is also interesting to point out that the nonuniform relative acceleration of the metal and the sphere will lead, at least in principle, in the Casimir oscillator of Sect. 8.2.2 to an additional damping mechanism associated with the parametric down-conversion of vibrational quanta into pairs of photons, a QED effect associated with the nonlinear properties of vacuum. This phenomenon, which was investigated theoretically by Lambrecht, Jackel, and Reynaud in the context of a vibrating parallel plate capacitor [120], is an example of the so called dynamical Casimir effect, i.e. the nonthermal radiation emitted by uncharged metal or dielectric bodies in a state of nonuniform acceleration [121] (see also the Chap. 13

of Dalvit et al. of this volume). The extraction of photons from vacuum in a cavity vibrating at twice the fundamental frequency of the cavity can be viewed as a parametric "vacuum squeezing" phenomenon. Physically, photons are created as a result of the time dependent boundary conditions of cavity modes, which produce electromagnetic fields. The observation of this effect would require a very high cavity Q ($\sim 10^8$–10^9) typical of superconductive cavities and GHz oscillations frequencies [120]. Such frequencies have been achieved in NEMS [122].

It is worth pointing out that radiation can be extracted from QED fluctuations also from a beam of neutral molecules interacting with a grating. In this case coherent radiation can be generated as result of the time dependent modulation of the Casimir-Polder-van der Waals force between the molecules and the grating. Radiation in the far infrared region should be attainable with beam densities of 10^{17} cm^{-3} [123].

8.6 Conclusions

In conclusion following a comprehensive state-of-the-art overview of the Casimir effect from its original proposal, we have discussed our recent and ongoing research in this promising field.

Note: A review has recently appeared [124] discussing the physics of the Casimir effect in microstructured geometries.

Acknowledgments The authors would like to thank D. Iannuzzi, M Lisanti, L Spector, M B Romanowsky, N Geisse, K Parker, R M Osgood, R Roth, H Stone, Y Barash, V A Aksyuk, R N Kleinman, D J Bishop for their collaborations and R Guerra, R Onofrio, M Kardar, R L Jaffe, S G Johnson, J D Joannopoulos, L Levitov, V Parsegian, J. N. Israelachvili, E Tosatti, V. Pogrovski, M Scully, P W Milonni, W. Kohn, M. Cohen, A Lambrecht, F. Intravaia, S. Reynaud for helpful suggestions and discussions.

References

1. Milonni, P.W.: The Quantum Vacuum: An Introduction to Quantum Electrodynamics. Academic Press, San Diego (1993)
2. Casimir, H.B.G.: On the attraction between two perfectly conducting plates. Proc. K. Ned. Akad. Wet. **60**, 793–795 (1948)
3. Casimir, H.B.G.: Haphazard Reality. Half a Century of Science. Harper and Row, New York (1983)
4. Jaffe, R.L., Scardicchio, A.: Casimir effect and geometric optics. Phys. Rev. Lett. **92**, 070402 (2004)
5. Scardicchio, A., Jaffe, R.L.: Casimir effects: an optical approach I. Foundations and examples. Nuc. Phys. B **704**, 552–582 (2005)
6. Sparnaay, M.J.: Measurements of attractive forces between flat plates. Physica **24**, 751–764 (1958)

7. van Blokland, P.H.G.M., Overbeek, J.T.G.: van der Waals forces between objects covered with a chromium layer. J. Chem. Soc. Faraday Trans. **74**, 2637–2651 (1978)
8. Lamoreaux, S.K.: Demonstration of the Casimir force in the 0.6 to 6 μm range. Phys. Rev. Lett. **78**, 5–8 (1997)
9. Mohideen, U., Roy, A.: Precision Measurement of the Casimir force from 0.1 to 0.9 μm. Phys. Rev. Lett. **81**, 4549–4552 (1998)
10. Roy, A., Lin, C.-Y., Mohideen, U.: Improved Precision Measurement of the Casimir force. Phys. Rev. D **60**, 111101 (1999)
11. Harris, B.W., Chen, F., Mohideen, U.: Precision Measurement of the Casimir force using gold surfaces. Phys.Rev. A **62**, 052109 (2000)
12. Ederth, T.: Template-stripped gold surfaces with 0.4-nm rms roughness suitable for force measurements: Application to the Casimir force in the 20–100 nm range. Phys. Rev. A **62**, 062104 (2000)
13. Bressi, G., Carugno, G., Onofrio, R., Ruoso, G.: Measurement of the Casimir force between parallel metallic surfaces. Phys. Rev. Lett. **88**, 041804 (2002)
14. Decca, R.S., Lopez, D., Fischbach, E., Krause, D.E.: Measurement of the Casimir Force between dissimilar metals. Phys. Rev. Lett. **91**, 050402 (2003)
15. Decca, R.S., Lopez, D., Fischbach, E., Klimchitskaya, G.L., Krause, D.E., Mostepanenko, V.M.: Precise comparison of theory and new experiment for the Casimir force leads to stronger constraints on thermal quantum effects and long-range interactions. Ann. Phys. **318**, 37–80 (2005)
16. Chan, H.B., Aksyuk, V.A., Kleinman, R.N., Bishop, D.J., Capasso, F.: Quantum mechanical actuation of microelectromechanical systems by the Casimir force. Sci. **291**, 1941–1944 (2001)
17. Derjaguin, B.V., Abrikosova, I.I.: Direct measurement of the molecular attraction of solid bodies. Statement of the problem and measurement of the force by using negative feedback. Sov Phys. JETP **3**, 819–829 (1957)
18. Milonni, Peter.W., Shih, Mei.-Li.: Casimir Forces. Contemp. Phys. **33**, 313–322 (1992)
19. Spruch, L.: Long-range (Casimir) interactions. Sci. **272**, 1452–1455 (1996)
20. Parsegian, V.A.: Van der Waals forces: a Handbook for Biologists. Chemists, Engineers, and Physicists, Cambridge University Press, New York (2006)
21. Mostepanenko, V.M., Trunov, N.N.: The Casimir effect and its applications. Oxford University Press, Clarendon NY (1997)
22. Milton, K.A.: The Casimir effect: Physical manifestations of zero-point energy. World Scientific, singapore (2001)
23. Bordag, M., Mohideen, U., Mostepanenko, V.M.: New developments in the casimir effect. Phys. Rep. **353**, 1–205 (2001)
24. Martin, P.A., Buenzli, P.R.: The Casimir effect. Acta Phys. Polon. B **37**, 2503–2559 (2006)
25. Lambrecht, A.: The Casimir effect: a force from nothing. Physics World **15**, 29–32 (2002). (Sept. 2002)
26. Lamoreaux, S.K.: Resource Letter CF-1: Casimir Force. Am. J. Phys. **67**, 850–861 (1999)
27. For an extensive bibliography on the Casimir effect see: http://www.cfa.harvard.edu/~babb/casimir-bib.html.
28. Lifshitz, E.M.: The theory of molecular attractive forces between solids. Sov Phys. JETP **2**, 73–83 (1956)
29. Dzyaloshinskii, I.E., Lifshitz, E.M., Pitaevskii, L.P.: The general theory of van der Waals forces. Adv. Phys. **10**, 165–209 (1961)
30. Lambrecht, A., Reynaud, S.: Casimir force between metallic mirrors. Eur Phys. J. D **8**, 309–318 (2000)
31. Klimchitskaya, G.L., Mohideen, U., Mostepanenko, V.M.: Casimir and van der Waals forces between two plates or a sphere (lens) above a plate made of real metals. Phys. Rev. A **61**, 062107 (2000)
32. Palik, E.D. (ed.): Handbook of Optical Constants of Solids. Academic, New York (1998)

33. Palik, E.D. (ed.): Handbook of Optical Constants of Solids: II. Academic, New York (1991)
34. Ordal, M.A., Bell, R.J., Alexander Jr., R.W., Long, L.L., Querry, M.R.: Optical properties of fourteen metals in the infrared and far infrared: Al, Co, Cu, Au, Fe, Pb, Mo, Ni, Pd, Pt, Ag, Ti, V, and W. Appl. Opt. **24**, 4493–4499 (1985)
35. Maradudin, A.A., Mazur, P.: Effects of surface roughness on the van der Waals force between macroscopic bodies. Phys. Rev. B **22**, 1677–1686 (1980)
36. Neto, P.A.M., Lambrecht, A., Reynaud, S.: Roughness correction to the Casimir force: Beyond the proximity force approximation. Europhys. Lett. **69**, 924–930 (2005)
37. Mahanty, J., Ninham, B.W.: Dispersion Forces. Academic, London (1976)
38. Israelachvili, J.N.: Intermolecular and Surface Forces. Academic, London (1991)
39. Henkel, C., Joulain, K., Mulet, J.Ph., Greffet, J.-J.: Coupled surface polaritons and the Casimir force. Phys. Rev. A **69**, 023808 (2004)
40. Intravaia, F., Lambrecht, A.: Surface plasmon modes and the Casimir energy. Phys. Rev. Lett. **94**, 110404 (2005)
41. Intravaia, F.: *Effet Casimir et interaction entre plasmons de surface*, PhD Thesis, Université Paris, (2005)
42. Lamoreaux, S.K.: Comment on Precision Measurement of the Casimir Force from 0.1 to 0.9 μm. Phys. Rev. Lett. **83**, 3340 (1999)
43. Lamoreaux, S.K.: Calculation of the Casimir force between imperfectly conducting plates. Phys. Rev. A **59**, 3149–3153 (1999)
44. Iannuzzi, D., Gelfand, I., Lisanti, M., Capasso, F.: New Challenges and directions in Casimir force experiments. Proceedings of the Sixth Workshop on Quantum Field Theory Under the Influence of External Conditions, pp. 11-16. Rinton, Paramus, NJ (2004)
45. Pirozhenko, I., Lambrecht, A., Svetovoy, V.B.: Sample dependence of the Casimir force. New J. Phys. **8**, 238 (2006)
46. Buks, E., Roukes, M.L.: Metastability and the Casimir effect in micromechanical systems. Europhys. Lett. **54**(2), 220–226 (2001)
47. Chan, H.B., Aksyuk, V.A., Kleinman, R.N., Bishop, D.J., Capasso, F.: Nonlinear micromechanical Casimir oscillator. Phys. Rev. Lett. **87**, 211801 (2001)
48. Iannuzzi, D., Lisanti, M., Munday, J.N., Capasso, F.: The design of long range quantum electrodynamical forces and torques between macroscopic bodies. Solid State Commun. **135**, 618–626 (2005)
49. de Man, S., Heeck, K., Wijngaarden, R.J., Iannuzzi, D.: Halving the Casimir force with conductive oxides. Phys. Rev. Lett. **103**, 040402 (2009)
50. Lisanti, M., Iannuzzi, D., Capasso, F.: Observation of the skin-depth effect on the Casimir force between metallic surfaces. Proc. Natl. Acad. Sci. USA **102**, 11989–11992 (2005)
51. Golestanian, R., Kardar, M.: ''Mechanical response of vacuum. Phys. Rev. Lett. **78**, 3421–3425 (1997)
52. Emig, T., Hanke, A., Kardar, M.: Probing the strong boundary shape dependence of the Casimir force. Phys. Rev. Lett. **87**, 260402 (2001)
53. Chan, H.B., Bao, Y., Zou, J., Cirelli, R.A., Klemens, F., Mansfield, W.M., Pai, C.S.: Measurement of the Casimir force between a gold sphere and a silicon surface with nanoscale trench arrays. Phys. Rev. Lett. **101**, 030401 (2008)
54. Parsegian, V.A., Weiss, G.H.: Dielectric anisotropy and the van der Waals interaction between bulk media. J. Adhes. **3**, 259–267 (1972)
55. Barash, Y.: On the moment of van der Waals forces between anisotropic bodies. Izv. Vyssh. Uchebn. Zaved. Radiofiz. **12**, 1637–1643 (1978)
56. Senturia, S.D.: Microsystem Design. Kluwer Academic, Dordrecht (2001)
57. Bishop, D.J., Giles, C.R., Austin, G.P.: The Lucent LambdaRouter MEMS: Technology of the future here today. IEEE Comun. Mag. **40**, 75–79 (2002)
58. Aksyuk, V.A., Pardo, F., Carr, D., Greywall, D., Chan, H.B., Simon, M.E., Gasparyan, A., Shea, H., Lifton, V., Bolle, C., Arney, S., Frahm, R., Paczkowski, M., Haueis, M., Ryf, R., Neilson, D.T., Kim, J., Giles, C.R., Bishop, D.: Beam-steering micromirrors for large optical cross-connects. J. Lightw. Technol. **21**, 634–642 (2003)

59. Serry, M., Walliser, D., Maclay, J.: The role of the Casimir effect in the static deflection and stiction of membrane strips in microelectromechanical systems (MEMS). J. Appl. Phys. **84**, 2501–2506 (1998)
60. De Los Santos, H.J.: Nanoelectromechanical quantum circuits and systems. Proc. IEEE **91**, 1907–1921 (2003)
61. Serry, F.M., Walliser, D., Maclay, G.J.: The anharmonic Casimir oscillator (ACO)-the Casimir effect in a model microelectromechanical system. J. Microelectromech. Syst. **4**, 193–205 (1995)
62. Landau, L.D., Lifshitz, E.M.: Mechanics. Pergamon, New York (1976)
63. Büscher, R., Emig, T.: Nonperturbative approach to Casimir interactions in periodic geometries. Phys. Rev. A **69**, 062101 (2004)
64. Klimchitskaya, G.L., Zanette, S.I., Caride, A.O.: Lateral projection as a possible explanation of the nontrivial boundary dependence of the Casimir force. Phys. Rev. A **63**, 014101 (2000)
65. Chen, F., Klimchitskaya, G.L., Mostepanenko, V.M., Mohideen, U.: Demonstration of the difference in the Casimir force for samples with different charge-carrier densities. Phys. Rev. Lett. **97**, 170402 (2006)
66. Iannuzzi, D., Lisanti, M., Capasso, F.: Effect of hydrogen-switchable mirrors on the Casimir force. Proc. Natl. Acad. Sci. USA **101**, 4019–4023 (2004)
67. Chu, W.K., Mayer, J.W., Nicolet, M.-A.: Backscattering Spectrometry. Academic Press, New York (1978)
68. Iannuzzi, D., Lisanti, M., Munday, J.N., Capasso, F.: Quantum fluctuations in the presence of thin metallic films and anisotropic materials. J. Phys. A: Math. Gen. **39**, 6445–6454 (2006)
69. Hough, D.B., White, L.R.: The Calcualtion of Hamaker constants from Lifshitz theory with applications to wetting phenomena. Adv. Colloid Interface Sci. **14**, 3–41 (1980)
70. Huiberts, J.N., Griessen, R., Rector, J.H., Wijngaarden, R.J., Dekker, J.P., de Groot, D.G., Koeman, N.J.: Yttrium and lanthanum hydride films with switchable optical properties. Nat. **380**, 231–234 (1996)
71. Richardson, T.J., Slack, J.L., Armitage, R.D., Kostecki, R., Farangis, B., Rubin, M.D.: Switchable mirrors based on nickel–magnesium films. Appl. Phys. Lett. **78**, 3047–3049 (2001)
72. de Man, S., Iannuzzi, D.: On the use of hydrogen switchable mirrors in Casimir force experiments. New J. Phys. **8**, 235 (2006)
73. de Man, S., Heeck, K., Wijngaarden, R.J., Iannuzzi, D.: Halving the Casimir force with conductive oxides. Phys. Rev. Lett. **103**, 040402 (2009)
74. Munday, J.N., Capasso, F.: Precision Measurement of the Casimir–Lifshitz force in a fluid. Phys. Rev. A **75**, 060102 (2007)
75. Munday, J.N., Capasso, F., Parsegian, V.A., Bezrukov, S.M.: Measurements of the Casimir–Lifshitz force in fluids: The effect of electrostatic forces and Debye the Casimir–Lifshitz force in fluids: The effect of electrostatic forces and Debye screening. Phys. Rev. A **78**, 032109 (2008)
76. Munday, J.N., Parsegian, V.A., Capasso, F.: Measured long-range repulsive Casimir–Lifshitz forces. Nat. **457**, 170–173 (2009)
77. Boyer, T.H.: 'Quantum electromagnetic zero-point energy of a conducting spherical shell and the Casimir model for a charged particle. Phys. Rev. **174**, 1764–1776 (1968)
78. Ambjorn, J., Wolfram, S.: Properties of the vacuum. I. mechanical and thermodynamic. Ann. Phys. **147**, 1–32 (1983)
79. Maclay, G.J.: Analysis of zero-point electromagnetic energy and Casimir forces in conducting rectangular cavities. Phys. Rev. A **61**, 052110 (2000)
80. Graham, N., Jaffe, R.L., Khemani, V., Quandt, M., Schroeder, O., Weigel, H.: The Dirichlet Casimir Problem. Nucl.Phys B **677**, 379–404 (2004)
81. Hertzberg, M.P., Jaffe, R.L., Kardar, M., Scardicchio, A.: Attractive Casimir forces in a closed geometry. Phys. Rev. Lett. **95**, 250402 (2005)

82. Tartaglino, U., Zykova-Timan, T., Ercolessi, F., Tosatti, E.: Melting and nonmelting of solid surfaces and nanosystems. Phys. Repts. **411**, 291–321 (2005)
83. Sabisky, E.S., Anderson, C.H.: Verification of the Lifshitz theory of the van der Waals potential using liquid-helium films. Phys. Rev. A **7**, 790–806 (1973)
84. Munday, J.N., Federico, C.: Repulsive Casimir and van der Waals forces: From measurements to future technologies. Inter. Journ. Mod. Phys. A **25**, 2252–2259 (2010)
85. Hutter, J.L., Bechhoefer, J.: Manipulation of van der Waals forces to improve image resolution in atomic-force microscopy. J. Appl. Phys. **73**, 4123 (1993)
86. Milling, A., Mulvaney, P., Larson, I.: Direct measurement of repulsive van der Waals interactions using an atomic force microscope. J. Col. Inter. Sci. **180**, 460 (1996)
87. Meurk, A., Luckham, P.F., Bergstrom, L.: Direct measurement of repulsive and attractive van der Waals forces between inorganic materials. Langmuir **13**, 3896 (1997)
88. Lee, S., Sigmund, W.M.: Repulsive van der Waals forces for silica and alumina. J. Col. Inter. Sci. **243**, 365 (2001)
89. Lee, S.W., Sigmund, W.M.: AFM study of repulsive van der Waals forces between teflon AF thin film and silica or alumina. Col. Surf. A **204**, 43 (2002)
90. Feiler, A., Plunkett, M.A., Rutland, M.W.: Superlubricity using repulsive van der Waals forces. Langmuir **24**, 2274 (2008)
91. Sader, J.E., et al.: Method for the calibration of atomic force microscope cantilevers. Rev. Sci. Instr **66**, 3789 (1995)
92. Cleveland, J.P., et al.: A nondestructive method for determining the spring constant of cantilevers for scanning force microscopy. Rev. Sci. Instr. **64**, 403 (1993)
93. Gibson, C.T., Watson, G.S., Myhra, S.: Scanning force microscopy—calibrative procedures for best practice. Scanning **19**, 564 (1997)
94. Craig, V.S.J., Neto, C.: In Situ calibration of colloid probe cantilevers in force microscopy: hydrodynamic drag on a sphere approaching a wall. Langmuir **17**, 6018 (2001)
95. Iannuzzi, D., Munday, J., Capasso, F.: Ultra-low static friction configuration. Patent submitted, (2005)
96. Ducker, W.A., Senden, T.J., Pashley, R.M.: Direct force measurements of colloidal forces using an atomic force microscope. Nat. **353**, 239–241 (1991)
97. van Enk, S.J.: Casimir torque between dielectrics. Phys. Rev. A **52**, 2569–2575 (1995)
98. Kenneth, O., Nussinov, S.: New polarized version of the Casimir effect is measurable. Phys. Rev. D **63**, 121701 (2001)
99. Shao, S.C.G., Tong, A.H., Luo, J.: Casimir torque between two birefringent plates. Phys. Rev. A **72**, 022102 (2005)
100. Torres-Guzmán, J.C., Mochán, W.L.: Casimir torque. J. Phys. A: Math. Gen. **39**, 6791–6798 (2006)
101. Rodrigues, R.B., Neto, P.A.M., Lambrecht, A., Reynaud, S.: Vacuum-induced torque between corrugated metallic plates. Europhys. Lett. **76**, 822 (2006)
102. Munday, J.N., Iannuzzi, D., Barash, Y., Capasso, F.: Torque on birefringent plates induced by quantum fluctuations. Phys. Rev. A **71**, 042102 (2005)
103. Munday, J.N., Iannuzzi, D., Capasso, F.: Quantum electrodynamical torques in the presence of brownian motion. New J. Phys. **8**, 244 (2006)
104. Prieve, D.C., Frej, N.A.: Total internal reflection microscopy: a quantitative tool for the measurement of colloidal forces. Langmuir **6**, 396–403 (1990)
105. Prieve, D.C.: Measurement of colloidal forces with TIRM. Adv. Colloid Interface Sci. **82**, 93–125 (1999)
106. Crocker, J.C., Grier, D.G.: Methods of digital video microscopy for colloidal studies. J. Colloid Interface Sci. **179**, 298–310 (1996)
107. Jones, R.C.: New calculus for the treatment of optical systems. I. Description and discussion of the calculus. J. Opt. A. **31**, 488–493 (1941)
108. Fowles, G.R.: Introduction to Modern Optics. Dover Publishing, New York (1968)

109. Levy, M., Osgood, R.M., Liu, R., Cross, L.E., Cargill III, G.S., Kumar, A., Bakhru, H.: Fabrication of single-crystal lithium niobate films by crystal ion slicing. Appl. Phys. Lett. **73**, 2293–2295 (1998)
110. Bimonte, G., Calloni, E., Esposito, G., Rosa, L.: Casimir energy and the superconducting phase transition. J. Phys. A: Math. Gen. **39**, 6161–6171 (2006)
111. Torricelli, G., van Zwol, P.J., Shpak, O., Binns, C., Palasantzas, G., Kooi, B.J., Svetovoy, V.B., Wuttig, M.: Switching Casimir forces with phase change materials. Phys. Rev. A **82**, 010101(R) (2010)
112. Soyka, F., et al.: Critical Casimir forces in colloidal suspensions on chemically patterned surfaces. Phys. Rev. Lett. **101**, 208301 (2008)
113. Sheehan, D.P.: Casimir chemistry. The J. Chem. Phys. **131**, 104706 (2009)
114. Cho, Y.K., et al.: Self-assembling colloidal-scale devices: selecting and using shortrange surface forces between conductive solids. Adv. Mater. **17**, 379 (2007)
115. Bishop, K.J.M., et al.: Nanoscale forces and their uses in self-assembly. Small **5**, 1600 (2009)
116. Levitov, L.S.: Van der Waals' friction. Europhys. Lett. **8**, 499–504 (1989)
117. Levitov L.S.: private communication
118. Pendry, J.B.: Shearing the vacuum-quantum friction. J. Phys.: Condens. Matter **9**, 10301–10320 (1997)
119. Kardar, M., Golestanian, R.: The friction of vacuum, and other fluctuation-induced forces. Rev Mod. Phys. **71**, 1233–1245 (1999)
120. Lambrecht, A., Jaekel, M., Reynaud, S.: Motion induced radiation from a vibrating cavity. Phys. Rev. Lett. **77**, 615–618 (1996)
121. Schwinger, J.: Casimir light: A glimpse. Proc. Natl. Acad. Sci. USA **90**, 958–959 (1993)
122. Huang, X.M.H., Feng, X.L., Zorman, C.A., Mehregany, M., Roukes, M.L.: VHF, UHF and microwave frequency nanomechanical resonators. New J. Phys. **7**, 247 (2005)
123. Belyanin, A., Kocharovsky, V., Kocharovsky, V., Capasso, F.: Coherent radiation from neutral molecules moving above a grating. Phys. Rev. Lett. **88**, 053602 (2002)
124. Rodriguez, A.W., Capasso, F., Johnson, S.G.: Nat. Photonics **5** 211 (2011)